



Enzymatic oxidation of polyethylene by *Galleria mellonella* intestinal cytochrome P450s

Jin-Soo Son^{a,1}, Soohyun Lee^{a,1}, Sungbo Hwang^b, Jinyoung Jeong^{c,d}, Seonghan Jang^a, Jiyoung Gong^{c,d}, Jae Young Choi^{f,g}, Yeon Ho Je^{e,f,g}, Choong-Min Ryu^{a,d,h,*}

^a Molecular Phytobacteriology Laboratory, Infectious Disease Research Center, KRIBB, Daejeon 34141 South Korea

^b Disease Target Structure Research Center, Division of Biomedical Research, KRIBB, Daejeon 34141 South Korea

^c Environmental Disease Research Center, KRIBB, Daejeon 34141, South Korea

^d KRIBB School, University of Science and Technology, 217, Daejeon 34113, South Korea

^e Department of Agricultural Biotechnology, College of Agriculture & Life Sciences, Seoul National University, Seoul 08826, South Korea

^f Research Institute for Agriculture and Life Sciences, Seoul National University, Seoul 08826, South Korea

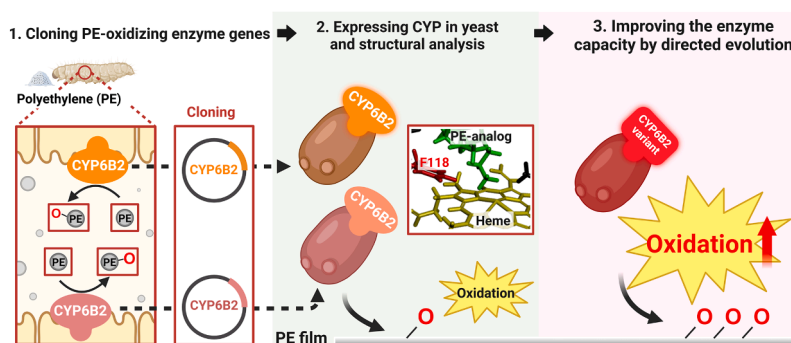
^g Center for Agricultural Microorganism and Enzyme, Seoul National University, Seoul 08826, South Korea

^h Department of Pediatrics, University of California at San Diego, La Jolla, CA, 92093-0380, USA

HIGHLIGHTS

- *Galleria mellonella* possesses intestinal enzymes that oxidize polyethylene (PE).
- CYP6B2-GP04 and CYP6B2-13G08 were identified as PE-oxidizing enzymes.
- Phe118 in CYP6B2-GP04 is critical for hydrocarbon interaction during PE oxidation.
- CYP6B2-GP04v1 had higher PE oxidation than the wild type after directed evolution.
- *G. mellonella* PE-oxidizing enzymes provide a green solution to biodegrade PE waste.

GRAPHICAL ABSTRACT



ARTICLE INFO

Keywords:

Cytochrome P450 monooxygenase
Galleria mellonella
Pichia pastoris
 Polyethylene oxidation
 Plastic biodegradation

ABSTRACT

Polyethylene is widely used but highly resistant to biodegradation, owing to its composition of only a hydrocarbon backbone. For biodegradation to occur, oxidation within the polymer needs to be initiated. *Galleria mellonella* was the first insect discovered to autonomously oxidize polyethylene without the aid of gut microbes. However, the specific enzyme remains unidentified. Here, we identified for the first time two polyethylene oxidation enzyme candidates of cytochrome P450 (CYP) 6B2-GP04 and CYP6B2-13G08 from the *G. mellonella* midgut. Both candidate clones oxidized polyethylene efficiently, generating short-chain aliphatic compounds, with CYP6B2-GP04 exhibiting higher activity than CYP6B2-13G08 in yeast and insect cells. *In silico* structural modeling approaches revealed that the CYP6B2-GP04 Phe118 was essential for interacting with hydrocarbons,

* Correspondence to: Molecular Phytobacteriology Lab, Korea Research Institute of Bioscience and Biotechnology (KRIBB), 125 Kwahak-ro, Daejeon 34141, South Korea.

E-mail address: cmryu@kribb.re.kr (C.-M. Ryu).

¹ These authors contributed equally to this work

<https://doi.org/10.1016/j.jhazmat.2024.136264>

Received 21 August 2024; Received in revised form 15 October 2024; Accepted 22 October 2024

Available online 23 October 2024

0304-3894/© 2024 The Author(s). Published by Elsevier B.V. This is an open access article under the CC BY license (<http://creativecommons.org/licenses/by/4.0/>).

which was further validated by mutating phenylalanine to glycine. Furthermore, directed enzyme evolution led to the identification of an enzyme variant with significantly increased oxidation efficiency. Our findings offer promising enzyme-based solutions for polyethylene biodegradation, potentially mitigating polyethylene-driven plastic pollution.

1. Introduction

Plastic is widely used in modern life in various forms, owing to its ease of processing, low weight, affordability, and strong durability [1]. However, ironically, the non-degradable nature of plastic has caused significant environmental issues [2,3]. Since 1950, global plastic production has been steadily increasing each year [4]. A recent report of Plastics Europe estimated that the production of plastic will reach approximately 33 billion tons by 2050 [5]. The Organisation for Economic Cooperation and Development (OECD) announced that polyethylene (PE) constituted the largest group (26.6 %) of total plastic waste compared with other plastic materials such as polypropylene (17.5 %), polyethylene phthalates (7.0 %), and polyvinyl chloride (6.0 %) in 2019 [6]. However, the absence of effective plastic waste management strategies and the low recycling rate of plastic have led to the accumulation of massive plastic waste, resulting in significant environmental issues [7,8]. Among plastics, PE is solely composed of a carbon-carbon (C–C) and carbon-hydrogen (C–H) backbone. The absence of hydrolysable groups within PE polymers renders them highly resistant to degradation. According to US Environmental Protection Agency data in 2015, only 9 % of PE waste was recycled in the US, while the majority ended up in landfills or was incinerated [9]. In addition, current chemical or mechanical recycling techniques face limitations due to low recovery efficiency or high energy demand and costs [10]. Moreover, PE incineration and chemical treatments generate toxic chemicals and greenhouse gases, leading to secondary detrimental effects on the environment and human health [11]. To overcome the fundamental problem of PE degradation, eco-friendly biodegradation technology is urgently required.

Plastic biodegradation refers to any physical or chemical change in a plastic polymer caused by biological processes, which are elicited by living organisms [12,13]. Since biodegradation is cost-effective and minimizes the generation of harmful byproducts, it has emerged as a prominent strategy for processing plastic residues [14]. In 2016, *Ideonella sakaiensis* 201-F6 was identified as the first microorganism possessing an enzyme, capable of degrading plastic materials. *I. sakaiensis* produces polyethylene terephthalatease (PETase) and mono (2-hydroxyethyl) terephthalate hydrolase (MHETase), which degrade PET and its intermediate, mono (2-hydroxyethyl) terephthalic acid, into terephthalic acid and ethylene glycol, respectively [15]. PET contains oxygen in its structure, which creates reactive sites that are targeted by specific enzymes, such as PETases. By contrast, PE is structurally stable and lacks reaction groups, which renders its biodegradation a significant challenge [16,17]. For PE biodegradation, oxidation is a critical initial step required to weaken its structural stability and make the polymer more susceptible to further breakdown [18,19]. Although some microbes, including the bacteria *Bacillus thuringiensis* and *B. subtilis*, and the fungi *Aspergillus fumigatus* and *A. flavus*, have been observed to macroscopically oxidize PE, the specific enzymes involved in PE oxidation remain unknown [19–22]. In 2014, the Indianmeal moth, *Plodia interpunctella*, was discovered to be capable of ingesting PE, prompting further studies on insect-driven PE oxidation [23–31]. Among the insect species reported to facilitate PE degradation, including *P. interpunctella*, *Zophobas atratus*, *Tenebrio molitor*, *Achroia grisella*, *Corcyra cephalonica*, and *Galleria mellonella*, the great waxworm *G. mellonella* has emerged as a particularly promising candidate for PE oxidation [23,26,28–30,32–37].

The high potential of *G. mellonella* to oxidize PE was first proposed in 2017. However, initial studies were limited to observing PE oxidation

using whole-body *G. mellonella* lysates, without attempting to identify the specific enzymes [28]. In 2019, Kong and colleagues demonstrated that PE oxidation in *G. mellonella* occurs independently of its gut microbiota, i.e., it is oxidized by endogenous *G. mellonella* enzymes [29]. In 2022, two hexamerins, Demetra and Ceres, were identified to be PE-oxidizing enzymes in salivary juice collected from the *G. mellonella* anterior digestive apparatus [36]. The following year, two additional hexamerins (Cibeles and Cora), capable of oxidizing PE, were discovered in *G. mellonella* saliva [38]. However, the oxidation of ingested PE in the digestive tract is potentially more critical, as the PE consumed by *G. mellonella* is swiftly transported from the mouth to the gut, where it can interact with various enzymes and undergo oxidation. Nevertheless, specific *G. mellonella* enzymes responsible for PE oxidation have not yet been identified.

Cytochrome P450 monooxygenases (CYPs) are a diverse class of enzymes, found in nearly all insect tissues. CYPs are essential for insect physiology, including the synthesis and degradation of juvenile hormone and ecdysteroids [39–42]. Furthermore, depending on the ecological niches, CYP enzymes have evolved the ability to oxidize and metabolize natural and synthetic chemicals, such as plant allelochemicals and insecticides [43–45]. Since insect CYPs pose significant obstacles to agriculture and human health, research has primarily focused on targeting their ability to detoxify insecticides [42,46–48]. On the other hand, *G. mellonella* naturally resides in beehives and mainly feeds on beeswax, which is composed of long-chain hydrocarbons and chemically similar to PE [29]. This implies that the CYP enzymes of *G. mellonella* may have acquired the ability to oxidize long-chain hydrocarbons. Indeed, transcriptomic analyses showed an increase in CYP450 gene expression after beeswax ingestion, indicating that these enzymes may be involved in metabolizing long-chain hydrocarbons [29]. However, whether they are involved in PE oxidation has not yet been investigated.

In this study, we discovered that orally ingested PE was primarily oxidized in the *G. mellonella* midgut, which led us to explore the presence of PE-oxidizing enzymes in the gut. Using forward- and reverse-genetics screening, we identified two efficient gut-derived PE-oxidizing enzymes, CYP6B2-GP04 and CYP6B2-13G08. Attenuated total reflection-Fourier transform infrared spectroscopy (ATR-FTIR) showed that both CYP6B2 enzymes effectively oxidized PE, causing the formation of C–O and C=O bonds within the PE polymer. In addition, gas chromatography-mass spectrometry (GC-MS) analysis revealed that the oxidized PE in the midgut was further metabolized into short aliphatic chains. *In silico* structural analysis and molecular docking simulations predicted the potential mechanism of action of gut-derived CYP450 enzymes and identified key residues crucial for PE oxidation. Targeted mutagenesis of these predicted key residues validated their crucial role in the ability of the enzyme to oxidize PE. Additionally, directed enzyme evolution generated enzyme variants with enhanced PE oxidation activities. The CYP6B2 enzymes discovered in this study are the first PE-oxidizing enzymes derived from the gut of *G. mellonella*, presenting a potential alternative for overcoming the challenge of PE oxidation in polyethylene degradation. Additionally, the PE-oxidizing enzyme screening method used in this study is expected to be useful for identifying other PE-oxidizing enzymes from various potential insect species known for their PE oxidation capabilities.

2. Methods

2.1. Insect rearing

G. mellonella larvae were obtained from the National Institute of Agricultural Sciences of Korea in 2013 and have been maintained under laboratory conditions. To maintain genetic diversity, wild-captured larvae were periodically introduced and bred together with the existing population. *G. mellonella* larvae were reared in $29.5 \times 23 \times 20.5$ -cm plastic cages (LocknLock, Seoul, South Korea) at 30°C within a plant growth chamber (Vision Tec Inc, Daegu, South Korea) under dark conditions and were fed an artificial waxworm diet consisting of wheat bran, glycerin, honey, and pollen, purchased from Sworm Farm (Cheonan, South Korea). To prevent fungal growth, the food was replaced weekly. When the larvae reached the final developmental stage (5 weeks old) and formed cocoons, they were transferred to new plastic cages and reared without food to prevent potentially pathogenic fungal growth. During this period, the larvae transitioned to the pupal stage and subsequently developed to adults. One week after emergence, adult *G. mellonella* began laying eggs on cage lids. The newly-laid eggs were carefully collected with tweezers and transferred to new plastic cages, containing the aforementioned artificial diet. Approximately two weeks later, the eggs hatched, and the larvae were reared to the adult stage as described above. Four-week-old larvae of similar body size were used in all experiments.

2.2. Attenuated total reflectance-Fourier transform infrared spectroscopy (ATR-FTIR) analysis

The oxidation within the PE polymer by the gut of *G. mellonella* and recombinant proteins produced by *P. pastoris* was analyzed using ATR-FTIR [28,29,49]. To evaluate PE oxidation in the *G. mellonella* gut during a single digestive cycle, 0.1 g PE powder was fed to 4 h-starved *G. mellonella* to allow them to naturally ingest PE. After 4 h, 50 *G. mellonella* larvae were rinsed with 100 % ethanol followed by sterile distilled water. Their entire guts were dissected. Gut samples were divided into foregut, midgut, and hindgut, as described by Sanger (2022) [50], and collected separately. The excreted *G. mellonella* PE-containing frass was collected separately. PE particles isolated from the gut and frass were treated with 40 % hydrogen peroxide (H_2O_2) at 60°C for 24 h to remove organic matter. This treatment effectively removed organic matter without altering the chemical structure or bonds of the PE (Fig. S1). After the removal of organic matter, PE particles were rinsed with 100 % ethanol and sterile distilled water, respectively. For ATR-FTIR analysis, the PE particles were collected by vacuum filtration using a Durapore® 0.45 μm PVDF membrane filter (Milipore Co. Burlington, MA, USA) and oven-dried at 60°C for 2 h.

PE oxidation by recombinant protein was evaluated using crude lysate from *P. pastoris* cells expressing the corresponding gene. Ten mL *P. pastoris* cell culture expressing a *G. mellonella*-derived gene was centrifuged at 1000 g at 4°C for 10 min. The cell pellet was resuspended in breaking buffer (50 mM sodium phosphate, pH 7.4, 1 mM EDTA, 5 % (v/v) glycerol) with Halt™ protease and phosphatase inhibitor cocktail (Thermo Scientific™, Waltham, MA, USA). *P. pastoris* cells were lysed by bead-beating with an equal volume of 425–600 μm acid-washed glass beads (Sigma-Aldrich, Burlington, MA, USA) (1:1, v/v) using a bead raptor 4 (OMNI International, Kennesaw, GA, USA). Fifty microliter of each *P. pastoris* cell lysate was applied to 10 mg of PE powder (Alfa Aesar Ward Hill, MA, USA). Fresh *P. pastoris* cell lysate was replaced 5 times at 1-h intervals to ensure effective oxidation of the PE. For ATR-FTIR analysis, the PE powder was washed with 40 % H_2O_2 followed by sterile distilled water to remove the cell debris, and then oven-dried at 60°C for 2 h. The oxidation within the PE polymer was analyzed using an ALPHA-P FTIR spectrometer equipped with an ATR crystal window (Bruker Optik GmbH, Ettlingen, Germany). Each analysis involved 64 scans per replicate covering a scan range of 4000 to 500 cm^{-1} with a

resolution of 4 cm^{-1} . ATR-FTIR analysis of each PE sample was performed in triplicate.

2.3. High-throughput screening system for PE oxidation with Micro-IR

The high-throughput screening system for PE oxidation by *Pichia pastoris* mutants using Micro-IR was performed according to Fig. S3. Cultures of *P. pastoris* transformants were transferred into a 96-well plate prefilled with 200 μL of Buffered Glycerol-complex (BMGY) broth medium (1 % yeast extract, 1.34 % YNB, 2 % peptone, 1 % glycerol, pH 6 100 mM sodium phosphate buffer, and 4×10^{-5} % biotin) and incubated for 2 days at 37°C . The plate was centrifuged at 1000 g for 5 min and the supernatant was removed. For recombinant protein expression, the cells were cultured in Buffered Methanol-complex (BMMY) (BMGY medium with 1 % glycerol having been by 0.5 % methanol) broth medium, and 1 % (v/v) methanol was added every 24 h for 2 days. To apply *P. pastoris* cell lysates on the PE film, the 96-well plate was centrifuged at 1000 g for 10 min at 4°C , and the pellets were resuspended in 25 μL sorbitol buffer (1 M sorbitol, 0.1 M Tris-HCl pH7.5), supplemented with 0.3 mg/mL zymolyase (Zymo Research, Orange, CA, USA), and Halt™ protease and phosphatase inhibitor cocktail (Thermo Scientific™, Waltham, MA, USA). For PE oxidation, 5 μL of *P. pastoris* cell lysate containing CYP6B2-GP04 was applied on the PE film, and the lysate was replaced with fresh *P. pastoris* cell lysates at 1 h intervals for a total of 5 applications. The PE film was washed with 40 % H_2O_2 , followed by sterile distilled water, to remove the cell debris. Oxidation within the PE film was analyzed using a Nicolet™ iN™10 Infrared Microscope (Thermo Scientific™, Waltham, MA USA) operated in ATR mode, which allowed the acquisition in the spectral range of $2000\text{--}500\text{ cm}^{-1}$ to detect C=O and C–O bonds.

2.4. Calculation of degradation indices

The degradation indices of PE were determined based on the ATR-FTIR spectrum as established by Almond (2020) [51], namely, by dividing the area of the carbonyl band ($1800\text{--}1650\text{ cm}^{-1}$), carbon-oxygen band ($1150\text{--}950\text{ cm}^{-1}$), or hydroxyl band ($3500\text{--}3300\text{ cm}^{-1}$) by a reference peak [51]. The reference peak used was the integrated band absorbance of methylene (CH_2) scissoring band ($1500\text{--}1420\text{ cm}^{-1}$). The peak area was calculated using Gaussian peak fitting in Origin 2023 [52].

2.5. Gas chromatography-mass spectroscopy (GC-MS) analysis

The metabolites resulting from PE degradation by the gut of *G. mellonella* and recombinant protein produced by *P. pastoris* were analyzed using a modified method of Zhang et al. (2022) [53]. To analyze gut metabolites following PE ingestion, guts of *G. mellonella* were collected after PE feeding for 4 h. PE metabolites were extracted from 0.2 g of gut sample using 10 mL of tetrahydrofuran. To analyze the PE metabolites produced by recombinant protein from *P. pastoris*, the PE particles was treated with 50 μL of *P. pastoris* cell lysate at 1 h intervals, and the procedure was repeated five times. After each treatment, the *P. pastoris* cell lysates were collected and pooled together. Collected *P. pastoris* cell lysates were mixed with 10 mL tetrahydrofuran to extract the PE metabolites. Each tetrahydrofuran mixture, containing either *G. mellonella* gut or *P. pastoris* cell lysate, was ultrasonicated at room temperature for 2 h and then concentrated using a Scan Vac Scanspeed vacuum centrifuge 40 (LaboGene, Hillerød, Denmark) to cause the solvent to evaporate. The concentrated extracts were redissolved by ultrasonication in 1 mL hexane for 20 min. For GC-MS analysis, the samples were filtered through a $0.22\text{-}\mu\text{m}$ PTFE filter (Agilent, Pal Alto, CA, USA). The PE metabolite profiles were analyzed using a 5975 C Agilent gas chromatograph (Agilent, Pal Alto, CA, USA) equipped with a HP-5MS column (30 m \times 0.25 mm-internal diameter and 0.25- μm width; Agilent) with helium as a carrier gas. One microliter of each

sample was injected. Initially, the oven temperature was set at 40 °C, it was increased by 10 °C/min until it reached 230 °C, and maintained at 230 °C for 2 min [29].

2.6. In silico structural analysis of CYP6B2-GP04

The complex structure of CYP6B2-GP04 and Heme was predicted by AlphaFold 3 [54]. The predicted complex structure was optimized by energy minimization in GROMACS [55] using the CHARMM36 force field. Using *in silico* alanine and glycine scanning mutagenesis, the structures of mutant proteins bearing a substitution of each of these seven key residues by an alanine or glycine were predicted using CHARMM-GUI based on the optimized wild-type structure of CYP6B2-GP04 [56]. The 3D structures of the eight differently-sized alkane structures, i.e., butane (PubChem CID: 7843), pentane (PubChem CID: 8003), hexane (PubChem CID: 8058), heptane (PubChem CID: 8900), octane (PubChem CID: 356), decane (PubChem CID: 15600), dodecane (PubChem CID: 8182), tetradecane (PubChem CID: 12389), were downloaded from Pubchem [57].

To generate the structures of complexes formed by the predicted CYP6B2-GP04 and the eight alkane molecules, molecular docking simulations were performed using AutoDock vina [58,59]. AutoDock vina uses the method of ligand-flexible docking simulations, a docking algorithm that involves changing the alkane molecule, and has a low calculation cost compared with AutoDock4 [60]. The binding site was defined by the ligand position on CYP3A4 (PDB ID: 6MA6) after superimposing the predicted structure with CYP3A4. Among the 10 binding configurations for each predicted CYP6B2-GP04 structure, binding poses were selected on the basis of the closest conformation of the ligand to the ferric ion in the heme structure. The hydrogen atoms in the predicted protein and ligand structures were added using Chimera 1.14 [61]. We also generated the structures of the complexes of CYP6B2-GP04 mutants, bearing substitutions of key residues to alanines or glycines, to superimpose their configurations to the one of the wild-type CYP6B2-GP04 protein upon PE polymer binding.

To predict the interaction energy between CYP6B2-GP04 and eight alkanes of different size, fragment molecular orbital (FMO) [62] calculations were performed using the predicted complex structures of CYP6B2-GP04 and the alkanes. The interaction energy predicted by FMO has been reported to be strongly correlated with experimental data [63]. Here, we performed all FMO calculations using the FMO-DFTB3 method [64]. Since the parameter related to the interaction between Fe and S is missing from the DFTB3 parameter set, the heme structure was removed from the structures of the complexes. All input files were prepared in compliance with the hybrid orbital projection fragmentation scheme [65]. The polarizable continuum model was used, and we considered that the alkane molecules bind to the receptors in solution [66]. The interaction energy was calculated by the sum of the pair interaction energy between the alkane ligand and all residues of the receptor protein. The FMO calculations were performed with the 30 June 2024 R1 GAMESS version [67].

2.7. Site-directed mutagenesis of CYP6B2-GP04

Site-directed mutagenesis of GP04 (Phe118Gly and Cys450Ala) was performed using overlap extension PCR. The procedure involved two rounds of PCR. In the first round, two separate PCR reactions were conducted using the pPICZα-A-CYP6B2-GP04 vector as the template and one mutagenic primer (Table S1), i.e., either GP04_BstBI-F or GP04_NotI-R. PCR products were purified using gel electrophoresis, and the desired DNA fragments were eluted using MinElute Gel Extraction Kit (Qiagen). The eluted fragments were used as templates for the second round of PCR, which employed the GP04_BstBI-F and GP04_NotI-R primers to amplify the full-length mutated CYP6B2-GP04 gene. The final PCR products were purified, digested with *BstBI* and *NotI*, and ligated into pPICZα-A vector using T4 DNA ligase. The ligated plasmid vectors were

transformed into DH5α competent *E. coli* cells. *P. pastoris* expressing mutant CYP6B2-GP04 was constructed by transforming 10 µg linearized plasmid vector as described above.

2.8. Direct evolution of CYP6B2-GP04 to improve PE oxidation through random mutagenesis

For the directed evolution of CYP6B2-GP04 through mutant library generation, error-prone PCR was conducted using the GeneMorph II Random Mutagenesis Kit (Agilent, Pal Alto, CA, USA) following the manufacturer's instructions, which specify the mutation frequency as 0–4.5 bp/kb. CYP6B2-GP04 was PCR-amplified using primers as described in Table S1. The PCR product was digested with *BstBI* and *NotI* and ligated into the pPICZα-A vector using T4 DNA ligase (Promega) according to the manufacturer's protocol. The ligation product was transformed to DH5α competent *E. coli* cells and incubated on LB agar plates supplemented with 50 µg/mL zeocin for 12 h at 37 °C. All colonies were scraped and further cultured in 50 mL LB broth supplemented with 50 µg/mL zeocin for 2 h. Plasmid vectors containing mutated CYP6B2-GP04 sequences were extracted using the Plasmid Midi Kit (Qiagen). *SacI*-linearized vectors were transformed into competent *P. pastoris* cells using electroporation, and *P. pastoris* transformants were incubated on YPD agar plates supplemented with 100 µg/mL zeocin for 48 h at 30 °C. Each colony was transferred to a 96-well microplate containing YPD broth, thus constructing a *P. pastoris* library encoding mutant CYP6B2-GP04. PE oxidation by the *P. pastoris* transformant library was analyzed using a high-throughput screening system with micro-FTIR. *P. pastoris* clones with increased PE oxidation were sequenced to identify the mutated regions within the CYP6B2-GP04 sequence.

2.9. Statistic analysis

The differential expression analysis in the transcriptomic study was analyzed using the Wald test. Analysis of qRT-PCR was performed by comparing the gene expression of the intestines of *G. mellonella* fed with PE and those under starvation versus the gene expression of intestines fed with artificial food. The qRT-PCR data were statistically analyzed using the Student's *t*-test. Degradation values including COI, CI, and HI values were analyzed using one-way analysis of variance (ANOVA) with Tukey's honestly significant difference (HSD) test. Differences were considered significant when *p*-values were < 0.05. Statistical analyses were performed, and graphs were plotted, using GraphPad Prism version 10.

3. Results

3.1. PE oxidation in the *G. mellonella* gut

To track the PE distribution in the gut after ingestion over time, fluorescently labeled PE particles were fed to *G. mellonella* larvae. Their location in the gut was observed under a fluorescence microscope. Despite individual variations, 1 h after PE feeding, the PE particles were primarily located in the foregut and anterior midgut (Fig. S2A). After 2 h, the PE particles were distributed throughout the midgut and hindgut, and continued to be detected up to 4 h after ingestion (Fig. S2A). Over time, the PE particles accumulated in the hindgut and were eventually excreted as frass (Fig. S2A). Similarly, 4 h after PE feeding, hematoxylin and eosin (H&E) staining of the gut revealed the presence of PE particles throughout the gut, with a greater abundance being observed in the midgut and hindgut, which indicated the rapid movement of ingested PE particles through the gut (Fig. 1A). By contrast, no debris was observed in the gut lumen of starved *G. mellonella* larvae (Fig. S2B).

To determine the specific gut location where oxidation of PE polymers occurred, PE particles were extracted from *G. mellonella* foregut, midgut, and hindgut 4 h after ingestion. Chemical modifications of PE polymers were examined using ATR-FTIR, and the results showed that

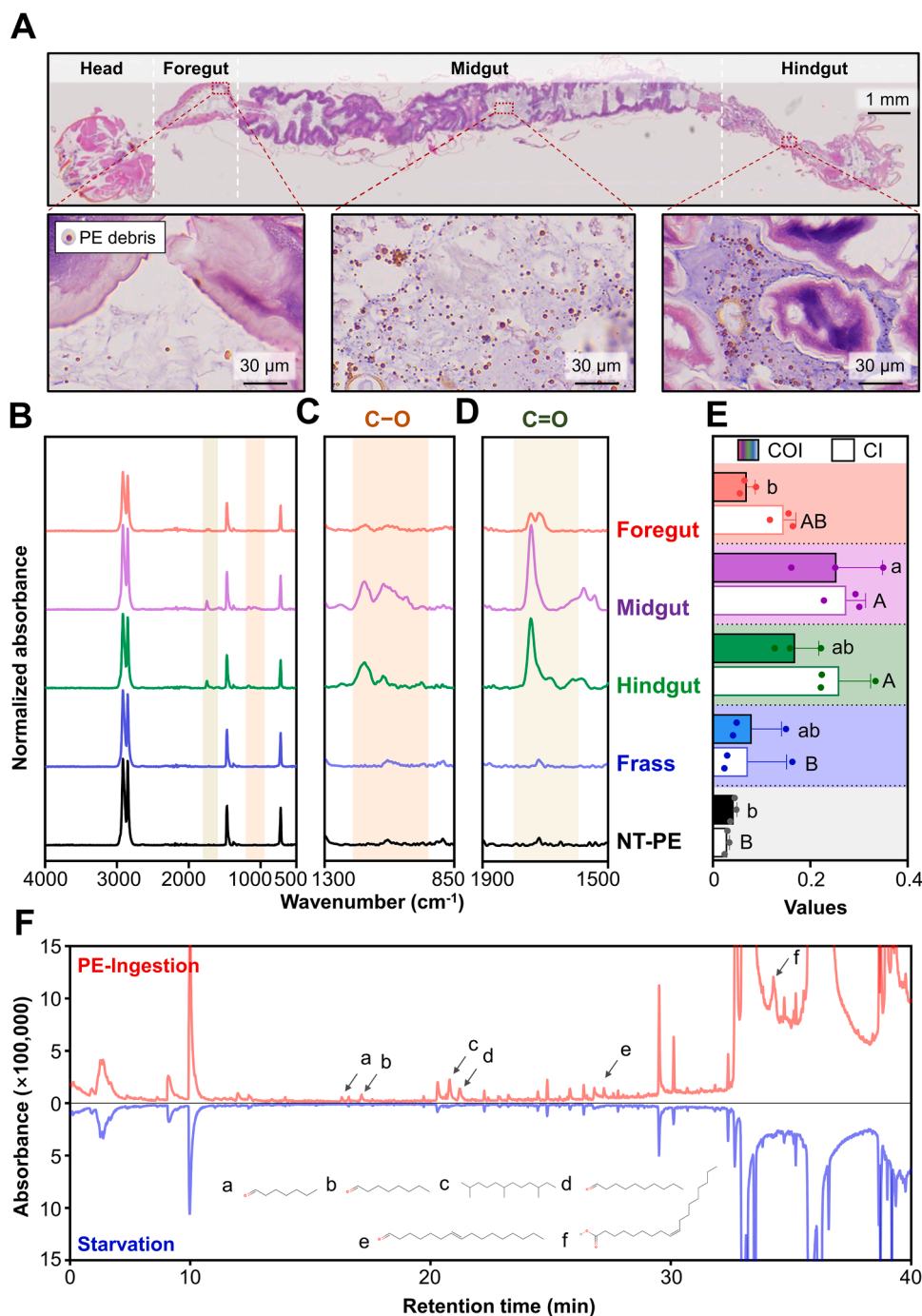


Fig. 1. *Galleria mellonella* can biologically oxidize polyethylene. (A) Hematoxylin and eosin staining of *G. mellonella* intestine 24 h after PE ingestion. Intestinal cells and structures are stained purple, and PE particles appear as reddish-brown circles. (B–D) FTIR spectrum (4000–500 cm^{-1}) of PE particles extracted from different sections of the *G. mellonella* intestine. (C) The beige-colored region highlights the 1200–950 cm^{-1} wavenumber range, in which C–O bonds are detected. (D) The sage-colored region marks the 1800–1600 cm^{-1} wavenumber range, indicative of C=O bonds. (E) Bar graph indicating the oxidation values of PE particles, isolated from different sections of the *G. mellonella* intestine and calculated based on their FTIR spectrum. The graph includes the carbon-oxygen (C–O) index (COI) and carbonyl (C=O) index (CI) values, which serve as quantitative measures of the extent of oxidation in PE particles. The CI value is represented by filled columns, whereas the COI value is represented by empty columns. One-way analysis of variance (ANOVA) was performed by Tukey's honestly significant difference (HSD) test. Different letters indicate statistically significant differences ($P \leq 0.05$). (F) GC-MS analysis of changes in gut metabolites in *G. mellonella* 4 h after PE ingestion. Different letters indicate newly formed metabolites and their chemical structures in the gut following PE ingestion.

oxidation of the PE polymer occurred throughout the gut, albeit at different levels (Fig. 1B–E). PE particles isolated from the foregut showed no significant difference in the carbon-oxygen index (COI) value, which indicated the formation of C–O bonds, compared with control PE particles (Fig. 1C and E). By contrast, PE particles isolated from the midgut exhibited 5.9-fold increases in COI value, compared

with control PE particles (Fig. 1C and E). PE particles isolated from the hindgut showed a 2.9-fold increase in COI value compared to control PE particles; however, this increase was not statistically significant (Fig. 1C and E). The carbonyl index (CI) value indicating C=O bonds significantly increased in PE particles from the gut of *G. mellonella*, showing a 9.3-fold increase in the midgut and a 5.6-fold increase in the hindgut,

compared to the control PE particles (Fig. 1D–E). In contrast, the CI value in PE particles isolated from the foregut showed a 4.9-fold increase compared to the control PE particles, but the increase was not statistically significant (Fig. 1D–E). The COI and CI values did not differ significantly between the PE collected from frass 4 h after ingestion and non-treated PE particles (Fig. 1C–E). The decrease in both values indicates that PE was actively oxidized within the *G. mellonella* gut, and after the PE was excreted as frass, no further PE oxidation could occur. In addition, oxidized PE could be subsequently degraded, leading to a

reduction in COI and CI values. GC-MS analysis revealed that ingested PE was oxidized and degraded into various aliphatic compounds in the *G. mellonella* gut, including acids, aldehydes, and hydrocarbons. The identified compounds included heptanal (16.3 min), octanal (17.1 min), 2,6,10-trimethyl dodecane (20.8 min), decanal (21.2 min), 2,4-dimethyl heptane (23.7 min), 7-hexadecenal (27.2 min), Z,Z-2,5-pentadecadien-1-ol (27.6 min), oleic acid (34.3 min), trans-13-octadecenoic acid (35.5 min), and 1-nonadecene (38.9 min) (Fig. 1F). By contrast, these aliphatic compounds did not exist in the gut of starved

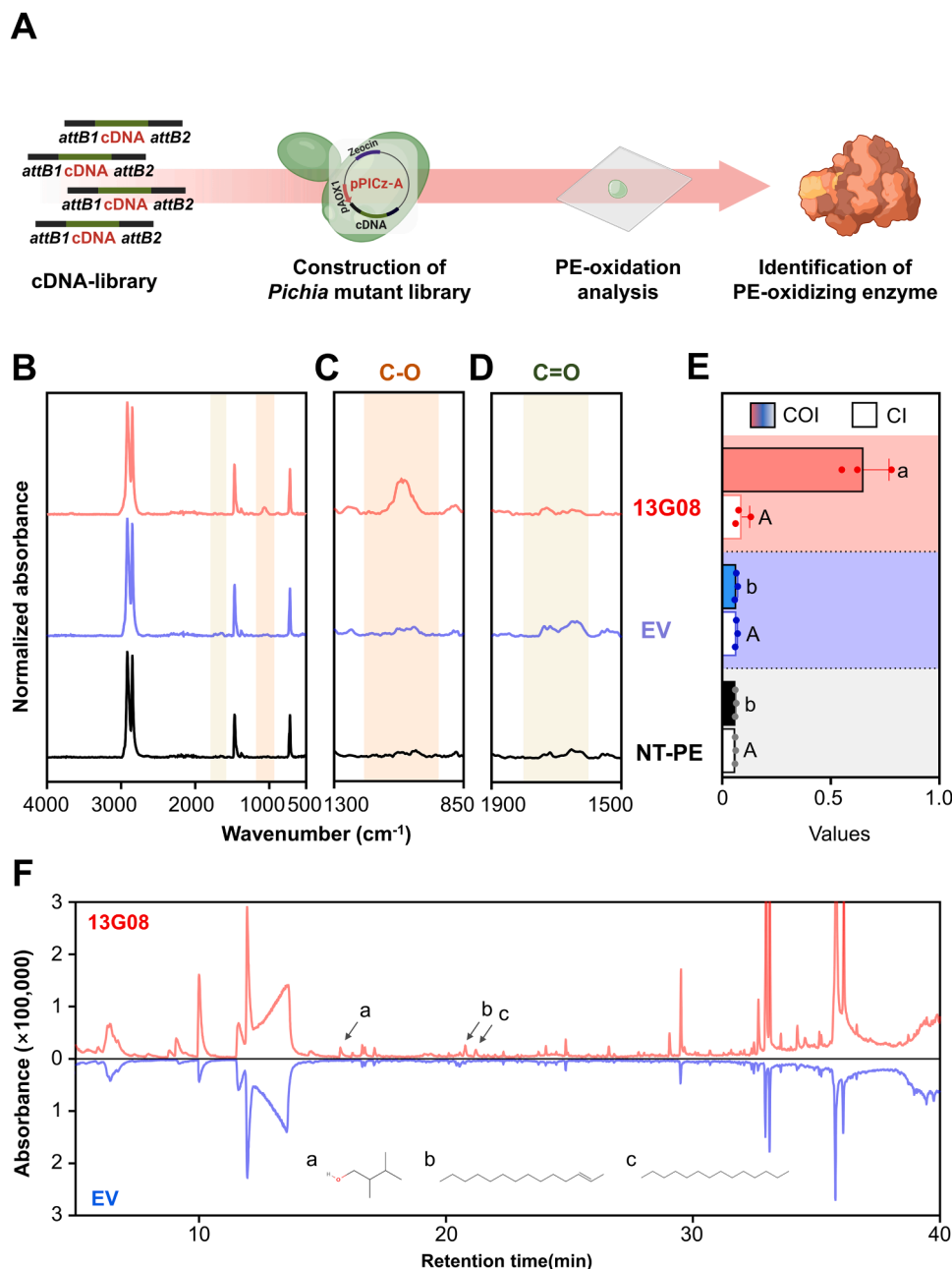


Fig. 2. Screening of the PE-oxidizing enzyme derived from the midgut of *G. mellonella* using forward genetic approaches. (A) Experimental scheme for exploring *G. mellonella* PE-oxidizing enzymes using the *P. pastoris* expression system and forward genetic screening. (B, C, D) FTIR spectrum of PE particles after their reaction with a *P. pastoris* cell lysate expressing CYP6B2-13G08, which was identified using forward genetic screening. (C) The beige-colored region highlights the wavenumber range of 1200–950 cm⁻¹, which corresponds to the detection of C–O bonds. (D) The sage-colored region marks the wavenumber range of 1800–1600 cm⁻¹, indicative of C=O bond detection. (E) The bar graph represents the oxidation values of PE particles calculated from the FTIR spectrum for each treatment. The CI value is represented by filled columns, whereas the COI value is represented by empty columns. One-way analysis of variance (ANOVA) was performed using the Tukey's honestly significant difference (HSD) test. Different letters indicate statistically significant differences ($P \leq 0.05$). (F) The GC-MS chromatogram shows the metabolites derived from PE oxidation by the *P. pastoris* cell lysate expressing CYP6B2-13G08. Different letters indicate newly formed metabolites and their chemical structures in the gut following PE ingestion.

G. mellonella (Fig. 1F). Taken together, our results demonstrate that PE oxidation actively occurs in the *G. mellonella* gut, especially the midgut and hindgut, leading to its further degradation into various metabolites.

3.2. Forward genetic screening to identify PE-oxidizing enzymes in *Pichia pastoris* as a eukaryotic surrogate host system

Expressing eukaryotic proteins in prokaryotic systems often faces limitations due to structural misfolding and loss of enzyme functionality, as prokaryotes lack the complex cellular machinery required for proper protein folding and post-translational modifications. To overcome these challenges, we employed the *Pichia pastoris* expression system (Fig. S3). This system allowed proper folding and post-translational modifications, enabling us to test the *G. mellonella*-derived protein for PE oxidation. Moreover, compared to the insect SF9 cell system, the *P. pastoris* expression system provided a more straightforward approach for introducing and expressing *G. mellonella* gut-derived genes, making it particularly effective for screening and identifying PE-oxidizing enzymes from *G. mellonella*.

Since PE oxidation in the midgut was drastically increased, we conducted a forward genetic screen to identify potential PE-oxidizing enzymes by cloning the cDNA library from the *G. mellonella* midgut into *E. coli* (Fig. 2A). A total of 1440 *E. coli* clones, each containing different *G. mellonella* cDNA fragments within the expression vector, were obtained. The cloned vectors were then transformed into *P. pastoris* to express the corresponding cDNA clones. The clones exhibiting PE oxidation effects were identified using a high-throughput screening system for PE oxidation, coupled with Micro-IR (Fig. S4). Among the *P. pastoris* clones obtained, only the 13G08 clone showed PE-oxidizing activity using ATR-FTIR analysis (Fig. 2B). Sequencing revealed that the 13G08 clone encodes an isoform of CYP6B2. To precisely evaluate the efficiency of PE oxidation by the CYP6B2 enzyme encoded by the 13G08 clone, its full-length cDNA coding sequence was cloned into the pPIC α -A expression vector and transformed into *P. pastoris*, with this enzyme designated as CYP6B2-13G08. The presence of the CYP6B2-13G08 enzyme in *P. pastoris* was confirmed by SDS-PAGE, and a 60-kDa protein was identified (Fig. S3B).

To verify the efficiency of PE oxidation by CYP6B2-13G08, 50 μ L of *Pichia* cell lysate was applied to 10 mg of PE particles in five separate treatments, each lasting 1 h (Fig. S3B). After a total reaction time of 5 h, the COI value of the treated PE particles increased significantly from 0.05 to 0.61 (Figs. 2B–C, and 2E). By contrast, the CI value did not increase significantly compared with untreated PE particles. Furthermore, the COI and CI values of PE particles treated with *P. pastoris* lysate harboring an empty vector (EV) showed no significant difference compared with the control non-treated PE particles (Fig. 2B–E). Unexpectedly, GC-MS analysis demonstrated that *P. pastoris* expressing CYP6B2-13G08 oxidized PE and produced various aliphatic compounds, including 2,3-dimethyl 1-butanol (14.3 min), 1-tetradecene (22.2 min), and tetradecane (22.4 min), despite not expressing other *G. mellonella* enzymes (Fig. 2F). *P. pastoris* harbors a variety of enzymes capable of metabolizing very long-chain fatty acids, similar to those of *G. mellonella* [68]. This suggests that after PE is oxidized by CYP6B2-13G08 expressed in *P. pastoris*, it can be further broken down by *P. pastoris* enzymes.

3.3. Transcriptome analysis during PE ingestion

To identify additional PE-oxidizing enzymes, we conducted transcriptome analysis of the *G. mellonella* midgut. RNA sequencing was conducted to identify candidate genes responsible for PE oxidation in larvae fed with PE for 24 h. Gene expression patterns were compared with those of larvae, fed with artificial food for 24 h, to allow enough time for gene expression alterations in response to PE ingestion to manifest. In addition, transcriptome analysis was performed on the midgut of larvae starved for 24 h to determine whether PE as the sole

nutrient source could provide sufficient nutrients to sustain metabolic processes.

Principal Component Analysis of the midgut transcriptome in PE- and (normal) food-fed insects revealed distinct gene expression patterns between the two groups, indicating that PE ingestion leads to gene expression alterations in the midgut (Fig. 3A). Interestingly, midguts of PE-fed insects exhibited similar gene expression patterns to those of starved insects (Figs. S5B–D). This finding is in agreement with our previous study, which indicated that ingesting PE alone causes *G. mellonella* to starve and lose weight owing to insufficient energy intake [29].

To identify midgut-derived enzymes involved in PE oxidation, we performed a differentially expressed gene analysis between food-fed and PE-fed insects using DESeq2. Transcripts were filtered using a fold change of > 2 , p -value of < 0.05 , and FDR of < 0.1 . In total, 1493 genes exhibited differential expression between PE-fed and food-fed insects (Fig. 3B). Among these, 1122 genes were downregulated, but 371 genes were upregulated in the midgut in response to PE ingestion (Fig. 3B). Functional annotation of the upregulated genes using the Clusters of Orthologous Groups of proteins (COGs) database revealed that the majority of them had currently unknown functions (Fig. S5A). However, among the known functions, 22 genes were associated with lipid metabolism, whereas 19 genes are involved in the biosynthesis, transport, and catabolism of secondary metabolites (Fig. 3C–D). These functions could play a crucial role in oxidation and further biodegradation of PE in the *G. mellonella* larval midgut.

Notably, the upregulated genes associated with the biosynthesis, transport, and catabolism of secondary metabolites included CYP enzymes, such as CYP4D1, CYP4V2, CYP6B2, CYP6B4, and CYP9F2, along with four variants of CYP4C1, denoted as CYP4C1-1, CYP4C1-2, CYP4C1-3, and CYP4C1-4 (Fig. 3C). The CYP monooxygenases are known to catalyze reactions including C–H hydroxylation, C=C bond epoxidation, and C–C bond cleavage. We previously demonstrated that CYP enzymes were involved in the metabolism of beeswax, which consists of long-chain hydrocarbons structurally similar to PE; therefore, CYP enzymes could play a crucial role in PE oxidation in the midgut of *G. mellonella* larvae [29].

Upregulated genes associated with lipid metabolism in response to PE ingestion could be involved in breaking down CYP-mediated oxidized PE in the larval *G. mellonella* midgut (Fig. 3D). The upregulation of lipase and esterase genes may be crucial for degrading long-chain esters formed during the in-chain oxidation of PE polymers by CYP enzymes. The upregulation of the *acyl-CoA oxidase 1* (*ACOX1*) and *oxidoreductase* genes, which initiate β -oxidation, indicates that long-chain acyl-CoA generated from long-chain fatty acids may be further processed through the β -oxidation metabolic pathway [69,70]. Upregulation of the *ATP-binding cassette subfamily A3* (*ABCA3*) could facilitate the transport of very-long-chain fatty acids derived from oxidized PE in the peroxisome, where β -oxidation occurs, potentially aiding in their breakdown [71,72]. Furthermore, increased expression of *short-chain dehydrogenase/reductase family 16 C member 6* (*SDR16C6*) indicates the presence of enhanced metabolism of short-chain fatty acids produced by β -oxidation [73].

Based on transcriptomic data, we identified eight CYP genes potentially involved in PE oxidation. However, their expression levels were also significantly increased under starvation conditions (Fig. S5C). The increase in expression levels may have occurred because CYP genes assist in fatty acid oxidation and stress regulation during starvation (Fig. S5D). Therefore, to identify CYP enzymes specifically involved in PE oxidation, the expression levels of these eight CYP genes were further validated at a short interval after PE ingestion (4 h), as well as after 24 h. Among them, CYP6B2-GP04 showed a significant increase in expression within 4 h after PE ingestion, coinciding with the duration of a single digestive cycle (Fig. 3E and Figs. S6A–H).

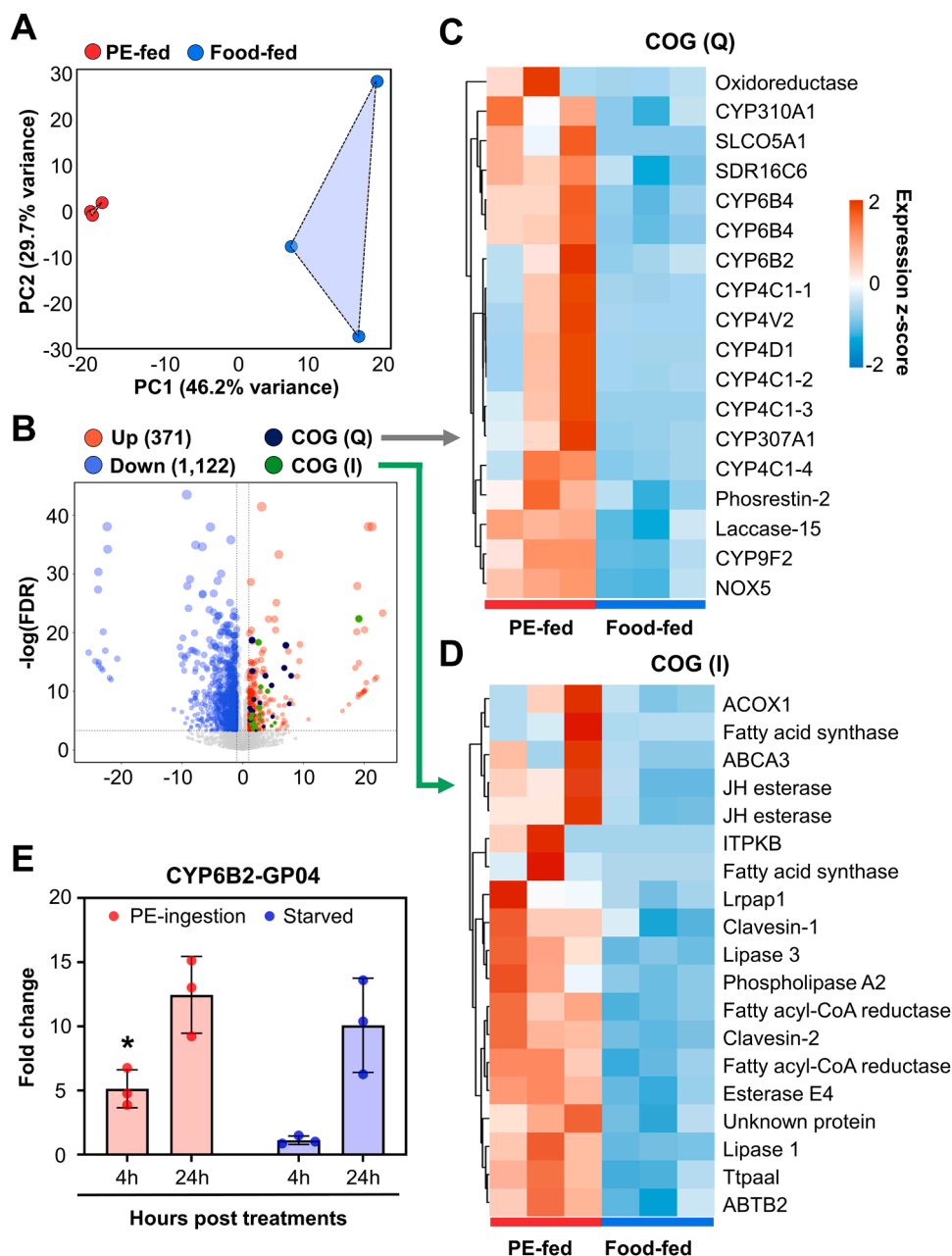


Fig. 3. Alteration of gene expression in the *G. mellonella* midgut following PE ingestion. (A) Principal component analysis (PCA) of transcriptomes from *G. mellonella* midguts. The analysis includes samples from *G. mellonella*, fed with PE and artificial waxworm diet. (B) Volcano plot depicting DEGs. Red dots mark the upregulated genes, whereas blue dots mark the downregulated genes after PE ingestion. Black dots indicate upregulated genes classified under COG (Q), whereas green dots indicate upregulated genes classified under COG (I). The x-axis is a \log_2FC representation of individual genes, and the y-axis represents their $-\log_{10}FDR$. (C, D) Heatmap indicating the DEGs related to the biosynthesis, transport, and catabolism of secondary metabolite function (C) and lipid metabolism (D) after PE ingestion. (E) RT-qPCR validation of CYP6B2-GP04 gene expression, performed at 4 h and 24 h after PE ingestion and starvation. Analysis of qRT-PCR was performed by comparing the gene expression of the intestines of *G. mellonella* fed with PE and those under starvation versus the gene expression of intestines fed with artificial food. The qRT-PCR data were statistically analyzed using the Student's *t*-test. The data presented are the mean \pm SD. The asterisk (*) indicates a statistically significant difference ($P \leq 0.05$).

3.4. PE oxidation activity of CYP6B2-GP04 in *P. pastoris*

To verify the PE oxidation activity of the gene identified by a reverse genetic approach based on transcriptomic analysis, the CYP6B2-GP04 gene was mutated and expressed in *P. pastoris* (Fig. 4A and Fig. S3A). SDS-PAGE analysis of the cell lysate from *P. pastoris* heterologously expressing CYP6B2-GP04 revealed a specific band at 58 kDa, corresponding to CYP6B2-GP04 (Fig. S3B).

ATR-FTIR analysis of the PE particles co-incubated with *P. pastoris* cell lysate, in which CYP6B2-GP04 had been expressed, revealed that the

COI of the treated PE particles increased significantly from 0.05 to 0.71 (Fig. 4B–C, and E). In addition, the CI value of the CYP6B2-GP04-treated PE particles increased 5.4-fold compared with the control PE particles (Figs. 4B, 4D, and 4E). By contrast, PE treated with *P. pastoris* cell lysate harboring an EV did not show significant differences in either CI or COI compared with untreated PE particles, which confirmed that the formation of C–O bonds in PE is specifically due to the activity of CYP6B2-GP04, rather than *P. pastoris* endogenous enzymes (Fig. 4B–E). In addition, GC-MS analysis detected various aliphatic compounds including hydrocarbons, acid and alcohol, such as 4-methyl octane

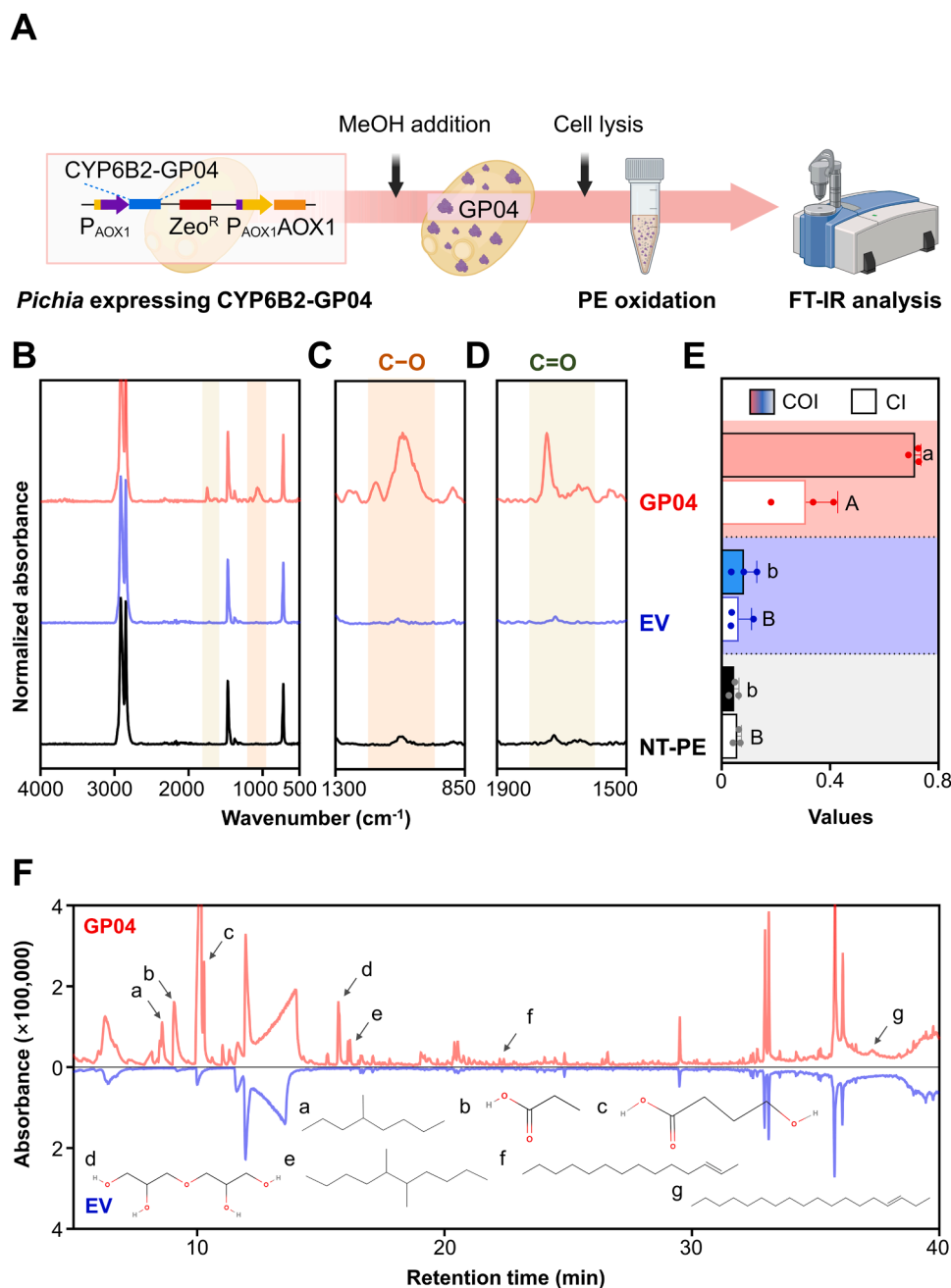


Fig. 4. Identification of the PE-oxidizing enzyme derived from the midgut of *G. mellonella* using a reverse-genetics approach. (A) Experimental scheme for the investigation of PE oxidation by *G. mellonella* intestine-derived enzymes using the *P. pastoris* expression system. (B–D) FTIR spectrum (4000–500 cm⁻¹) of PE particles after reaction with CYP6B2-GP04. (C) The beige-colored region marks the wavenumber range of 1200–950 cm⁻¹, in which C–O bonds are detected. (D) The sage-colored region indicates the wavenumber range of 1800–1600 cm⁻¹, in which C=O bonds are detected. (E) The bar graph represents the oxidation values of PE particles calculated from the FTIR spectrum for each treatment. The CI value is represented by filled columns, whereas the COI value is represented by empty columns. One-way analysis of variance (ANOVA) was performed by Tukey's honestly significant difference (HSD) test. Different letters indicate statistically significant differences ($P \leq 0.05$). (F) The GC-MS spectrum shows the metabolites derived from PE oxidation using a *Pichia* cell lysate expressing CYP6B2-GP04. Different letters indicate newly formed metabolites and their chemical structures in the gut following PE ingestion.

(8.6 min), propanoic acid (9.1 min), 4-hydroxy butanoic acid (10.2 min), 1-methylhexyl hydroperoxide (11.3 min), 4,5-diethyl octane (15.3 min), diglycerol (15.7 min), 5,6-dimethyl decane (16.1 min), (E)–2-tetradecene (22.2 min), tetradecane (22.4 min), 2-methyl hexadecanol (26.4 min), 7-methyl-Z-tetradecen-1-ol acetate (28.4 min), and 3-octadecene (37.3 min), after treatment with *P. pastoris* expressing CYP6B2-GP04 (Fig. 4F). This suggests that PE oxidized by CYP6B2-GP04 undergoes further degradation by yeast-derived enzymes. Although CYP6B2-GP04 and CYP6B2–13G08 are both isomers of CYP6B2, their

activities in oxidizing PE appeared to differ. Compared with treatment with CYP6B2–13G08, PE treated with CYP6B2-GP04 exhibited higher COI and CI values (Fig. 2E and Fig. 4E). In addition, the number and types of organic metabolites were higher in PE treated with CYP6B2-GP04, indicating that the PE-oxidation activity of CYP6B2-GP04 might be higher than that of CYP6B2–13G08 (Fig. 2F and Fig. 4F). However, CYP6B2–13G08 showed significantly higher expression levels upon PE ingestion (Fig. S6I), suggesting that CYP6B2–13G08 can effectively oxidize PE, despite having lower oxidation efficiency than CYP6B2–

GP04.

3.5. Phylogenetic analysis of CYP6B2 homologous enzymes

A meta-analysis of the NCBI database revealed that CYP6B2 enzymes are uniquely found within the order Lepidoptera [39,74]. Phylogenetic analysis revealed that the *G. mellonella* CYP6B2 enzymes have evolved distinctly from other herbivorous insect species such as *Cydia*, *Ostrinia*,

and *Spodoptera*. Instead, the CYP6B2 enzymes of *G. mellonella* cluster closely with those of the lesser wax moth, *A. grisella*, which is also a honeybee colony pest (Fig. S7). The clustering pattern suggests that the evolutionary functional divergence of CYP6B2 enzymes may be closely linked to the dietary habits of insect species. Analysis of conserved motif variations in CYP6B2 revealed that *G. mellonella* CYP6B2 enzymes are divided into three distinct clades (Fig. S7). CYP6B2-GP04 and CYP6B2-13G08 are classified into two different clades, indicating the

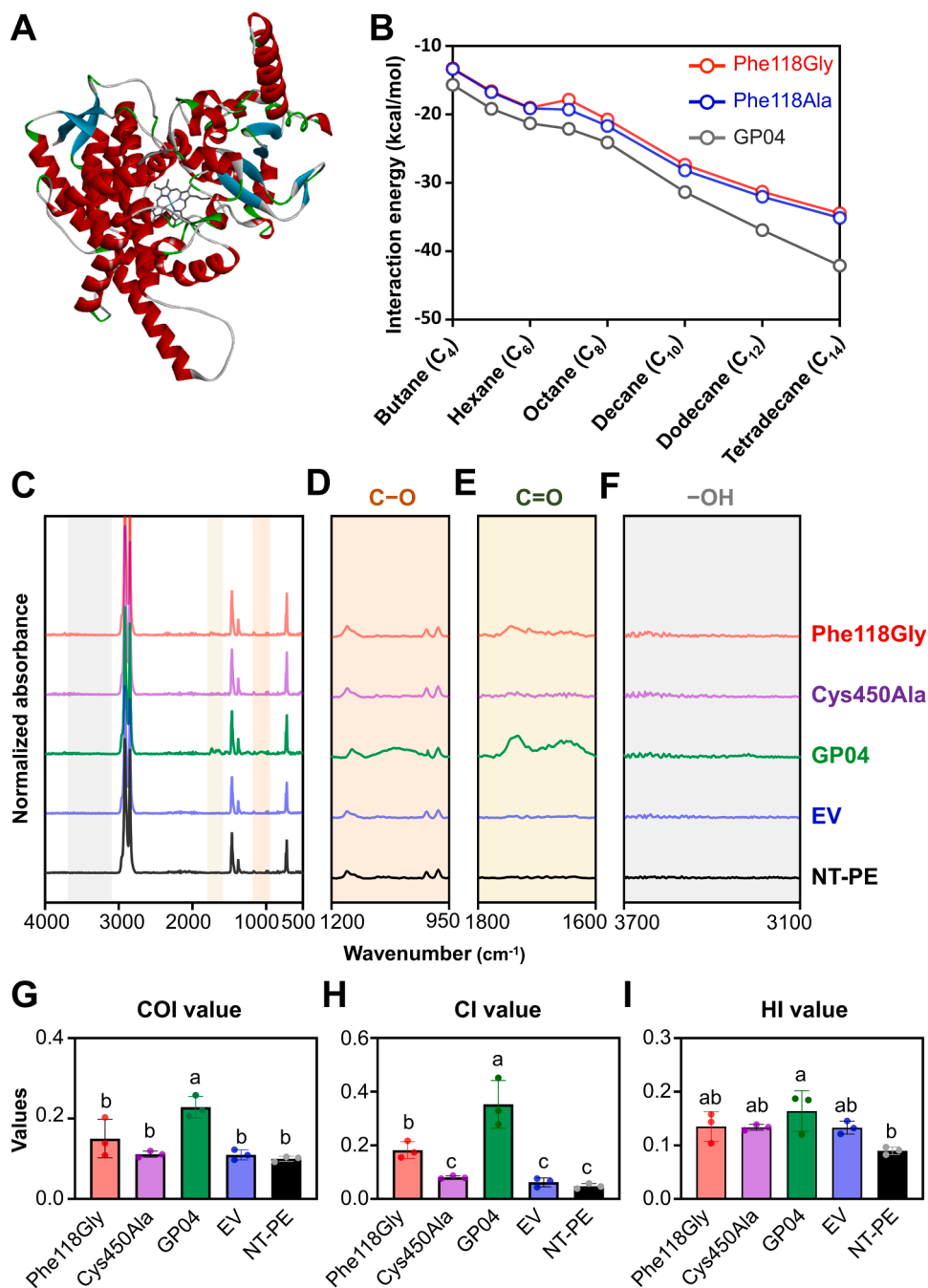


Fig. 5. *In silico* structural analysis of the interaction of CYP6B2-GP04 with hydrocarbons. (A) CYP6B2-GP04 structural prediction using AlphaFold3. (B) Interaction energy between the wild-type CYP6B2-GP04 and CYP6B2-GP04 mutant variants. The interaction energy was predicted using the FMO-DFTB3 method and calculated as the sum of interaction energies of the alkane ligands and all the residues of the receptor protein. (C) FTIR spectrum (4000–500 cm⁻¹) of PE films, after their reaction with the wild-type CYP6B2-GP04 and the Phe118Gly variant. The beige-colored area indicates the wavenumber range of 1200–950 cm⁻¹, in which C–O bonds are identified. The sage-colored area highlights the wavenumber range of 1800–1600 cm⁻¹, which signifies the presence of C=O bonds. The gray-colored area marks the wavenumber range of 3700–3100 cm⁻¹, which corresponds to the detection of hydroxyl bond (-OH). (D–F) Bar graph representing the COI (G), CI (H), and hydroxy index (HI) (I) values, calculated based on the FTIR spectrum. One-way analysis of variance (ANOVA) was performed using the Tukey's honestly significant difference (HSD) test. Different letters indicate statistically significant differences ($P \leq 0.05$).

existence of phylogenetic and functional differences between them (Fig. S7), as well as potential variations in their functions and polyethylene oxidation mechanisms.

3.6. Validation of PE oxidation activity of CYP6B2 in insect cells

The CYP6B2 enzyme is specific to Lepidoptera. To verify the PE oxidation activity of the two identified *G. mellonella* CYP6B2 enzymes in cells of insect origin, CYP6B2-GP04 and CYP6B2-13G08 genes were expressed in the Sf9 insect cell line, which is derived from the lepidopteran *Spodoptera frugiperda*. SDS-PAGE analysis confirmed the sizes of the CYP6B2-GP04 and CYP6B2-13G08 proteins to be 58 kDa and 60 kDa, respectively, which matched the protein sizes expressed in *P. pastoris* cells (Figs. S8A–B). Sf9 cells expressing each CYP6B2 enzyme were completely sonicated. The cell lysates were incubated with 10 mg of PE particles, treated in five intervals of one-hour each. After 5 h of incubation, PE particles treated with Sf9 cells expressing CYP6B2-GP04 formed C–O, C=O, and hydroxyl (–OH) bonds in the PE polymer (Figs. S8C–F). Specifically, for PE particles treated with CYP6B2-GP04, the COI increased significantly from 0.09 to 0.33, and the CI increased from 0.12 to 0.57, compared with untreated PE particles. However, the hydroxyl index (HI) did not show a significant increase (Figs. S8G–I). By contrast, the PE film treated with CYP6B2-13G08 showed a significant increase in CI from 0.012 to 0.30 compared with untreated PE, whereas its COI and HI values were not significantly increased. Similar to the results observed with the *P. pastoris* expression system, in the insect Sf9 cell expression system, the degree of oxidation by CYP6B2-13G08 was significantly lower compared to CYP6B2-GP04, indicating that CYP6B2-13G08 has lower PE oxidation activity than CYP6B2-GP04. PE particles treated with Sf9 cells (Mock) and Sf9 cells containing the EV showed no difference in COI, CI, or HI values compared with untreated PE. These results confirm that CYP6B2 enzymes derived from the gut of *G. mellonella* are indeed active when expressed in insect cell lines, demonstrating the same PE oxidation activity as when expressed in *P. pastoris*.

3.7. In silico structural modeling of PE-oxidizing CYP6B2-GP04

The CYP6B2-GP04 and CYP6B2-13G08 structure containing the heme structure were predicted and constructed using AlphaFold3 (Fig. 5A and Fig. S9A). Pairwise alignment of the amino acid sequences of CYP6B2-GP04 and CYP6B2-13G08 using the SIM program revealed a similarity of 36.5 %. Nevertheless, the two CYP6B2 proteins were found to be structurally similar. The predicted structures of CYP6B2-GP04 and CYP6B2-13G08 were confirmed to have high structural similarity to human CYP3A4 and CYP3A5 using Swiss-Model. Additionally, structural superposition analysis using Chimera revealed that CYP6B2-GP04 and CYP6B2-13G08 share significant structural similarity with each other, and that CYP6B2-GP04 also exhibits notable structural resemblance to human CYP3A4 (Figs. S9B–C). Although the substrate binding and oxidizing mechanisms of CYP6-family enzymes have not yet been fully elucidated, the observed structural similarities suggest that the structure of CYP6B2-GP04 and CYP6B2-13G08 in complex with its substrate may operate in a manner akin to human CYP3A4 and CYP3A5. Among the two PE-oxidizing CYP6B2 enzymes, we focused on CYP6B2-GP04 for subsequent structural experiments due to its higher PE oxidation activity compared with CYP6B2-13G08, aiming to identify its key structural features and potential interactions with hydrocarbons. To predict the complex structures of CYP6B2-GP04 and CYP6B2-13G08 with the PE polymer, molecular docking simulations were performed using hydrocarbons of various lengths (C_{4–14}) as structural analogs of PE.

The predicted structure of CYP6B2-GP04 interacted more strongly with longer hydrocarbons; the interaction energy decreased from –15.68 kcal/mol for butane (C₄) to –42.10 kcal/mol for tetradecane (C₁₄) (Fig. 5 and Fig. S10). Similarly, for CYP6B2-13G08, the interaction

energy also decreased as hydrocarbon length increased, from –14.21 kcal/mol with butane (C₄) to –33.32 kcal/mol with tetradecane (C₁₄) (Fig. S10). The decrease in interaction energy with longer hydrocarbons indicates that CYP6B2-GP04 and CYP6B2-13G08 bind more effectively to longer hydrocarbons, supporting the finding that both CYP6B2 enzymes can efficiently oxidize PE. To predict key residues related to interaction energy, fragment molecular orbital (FMO) calculations were performed using the predicted structures of CYP6B2-GP04 and CYP6B2-13G08 complexes with C_{4–14} hydrocarbons. Seven key residues in CYP6B2-GP04—Arg104, Phe118, Phe213, Val306, Ala310, Thr314, and Ile490—were predicted to be important for binding to various hydrocarbons. Similarly, the residues Phe118, Phe210, Val309, Ala313, Thr314, Ile494, and Val495 in CYP6B2-13G08 were identified as important for binding to C_{4–14} hydrocarbons. In both two CYP6B2 enzymes, Phe118 was predicted to be the most important for interacting with the PE polymer. Due to the structural similarity between the two PE-oxidizing CYP6B2 enzymes, we focused on CYP6B2-GP04, which exhibits higher PE oxidation activity than CYP6B2-13G08, for subsequent experiments.

3.8. Identification and validation of key residues required for PE oxidation

To pinpoint the CYP6B2-GP04 key residues involved in binding PE, an *in silico* mutagenesis experiment was conducted. Alanine and glycine scanning mutagenesis were performed on seven residues identified from the binding assay of CYP6B2-GP04 with C_{4–14} hydrocarbons. In an *in silico* alanine mutagenesis screen, the variants Arg104Ala, Phe118Ala, Phe213Ala, and Thr314Ala exhibited increased interaction energy with C_{4–14} hydrocarbons compared with the wild-type CYP6B2-GP04 (Fig. S11A). Similarly, in an *in silico* glycine mutagenesis screen, the variants Phe118Gly, Phe213Gly, and Thr314Gly showed increased interaction energy with C_{4–14} hydrocarbons compared with the wild-type CYP6B2-GP04 (Fig. S11B). These specific amino acids are presumed to play crucial roles in the interactions between the enzyme and C_{4–14} hydrocarbons. Substitutions by alanines or glycines increased the interaction energies, indicating that these residues significantly contribute to the interaction energy and stability of the enzyme–substrate complex.

Among the seven residues, substitution of Phe118 with either alanine or glycine exhibited the greatest increase in interaction energy with C_{4–14} hydrocarbons (Fig. 5B). The Phe118Ala variant exhibited an increase in interaction energy ranging from 2.32 (C₄) to 6.98 (C₁₄) kcal/mol compared with the wild-type CYP6B2-GP04, whereas the Phe118Gly variant demonstrated an increase in interaction energy ranging from 2.40 (C₄) to 7.64 (C₁₄) kcal/mol. This significant increase highlights the importance of Phe118 in CYP6B2-GP04 for binding to C_{4–14} hydrocarbons. To further validate our computational findings, we generated a Phe118Gly mutant and expressed it in *P. pastoris*. We also expressed a Cys450Ala mutant, which cannot bind heme; since heme is required for substrate oxidation, this mutant cannot oxidize PE. To compare the efficiency of PE oxidation among CYP6B2-GP04, CYP6B2-GP04 Phe118Gly, and CYP6B2-GP04 Cys450Ala, expressed in *P. pastoris*, cell lysates were applied to PE films in five separate treatments, each lasting 1 h. ATR-FTIR analysis demonstrated that CYP6B2-GP04 Cys450Ala could not oxidize PE, which confirmed that PE oxidation depends on the presence of the heme group in the enzyme (Fig. 5C–J). The CYP6B2-GP04 Phe118Gly mutant exhibited a lower oxidation value compared with the wild-type CYP6B2-GP04 (Fig. 5G–I). While the wild-type CYP6B2-GP04 showed a significant increase in oxidation metrics with a COI value 2.1-fold higher and a CI value 4.4-fold higher compared with non-treated PE film, these values were markedly reduced in the presence of the Phe118Gly mutation (Fig. 5G–I). Specifically, the CYP6B2-GP04 COI decreased by 37.1 %, and CI decreased by 48.5 % compared with the wild-type CYP6B2-GP04, demonstrating a substantial decrease in the PE oxidation capacity in the

presence of the Phe118Gly mutation (Fig. 5G–I). These results underscore the critical role of Phe118 in the catalytic efficiency of CYP6B2-GP04 and suggest that modifications at this site have a significant impact on the functionality of the enzyme.

3.9. Improving PE oxidation capacity through directed evolution

To enhance the PE oxidation activity of CYP6B2-GP04, we performed error-prone PCR to randomly introduce 1–6 bp mutations into the *CYP6B2-GP04* coding sequence. The randomly mutated *CYP6B2-GP04* genes were cloned into the pPIC α -A expression vector and transformed into *P. pastoris* cells to generate yeast libraries expressing mutant CYP6B2-GP04 enzymes. A total of 1056 *P. pastoris* clones expressing mutant CYP6B2-GP04 were obtained. The PE oxidation activities of these clones were subsequently verified by incubating *P. pastoris* cell lysates with PE film using Micro-IR spectrophotometry. Among all the *P. pastoris* clones, a mutated enzyme named CYP6B2-GP04v1 exhibited higher PE oxidation activity compared with the wild-type CYP6B2-GP04 (Fig. 6A–D). FTIR analysis showed that the PE film treated with CYP6B2-GP04v1 had increased oxidation values compared with the PE film treated with the CYP6B2-GP04. Specifically, the COI value increased 1.4-fold, the CI value by 1.7-fold, and the HI value by 2.3-fold (Fig. 6E–G). Sequencing revealed that the CYP6B2-GP04v1 enzyme had mutations at four nucleotide positions, resulting in the following amino acid substitutions: Gly114Ala, Phe188Lys, Ala310Thr, and Glu400His.

To elucidate the differences in substrate interaction between CYP6B2-GP04 and CYP6B2-GP04v1, we conducted *in silico* molecular

docking simulations using C_{4-14} hydrocarbons, which are structurally similar to PE. Calculations of the interaction energy between C_{4-14} hydrocarbons and CYP6B2-GP04v1 revealed that the interaction energies with C_{7-10} hydrocarbons were approximately -1.38 to -0.63 kcal/mol lower than those with CYP6B2-GP04 (Fig. S12). The lower interaction energies suggests that the substrates bind more strongly to CYP6B2-GP04v1 than to CYP6B2-GP04. However, for C_{4-6} or C_{10-12} hydrocarbons, the interaction energy of wild-type CYP6B2-GP04 is lower than that of CYP6B2-GP04v1. Differences in interaction energy highlight the need for precise structural characterization of CYP6B2-GP04 and CYP6B2-GP04v1 to fully understand the increased PE oxidation effect observed with CYP6B2-GP04v1.

4. Discussion

Carbon oxidation within the PE polymer is a crucial initial step for PE decomposition, as it facilitates the breakdown of long hydrocarbon chains into smaller molecular fragments to enable further degradation [19,75]. PE oxidation using physical and chemical methods, such as thermal oxidation, UV-induced photooxidation, and chemical treatments with prooxidants, are commonly used but often result in incomplete degradation and formation of secondary pollutants [10]. Therefore, biological methods that are more sustainable and environmentally friendly, are emerging as promising alternatives for plastic waste reduction. Insects have recently attracted significant interest among living organisms, because insects constitute the most diverse group of animals and have been observed to consume PE, indicating that PE-oxidizing enzymes are potentially present in their digestive systems.

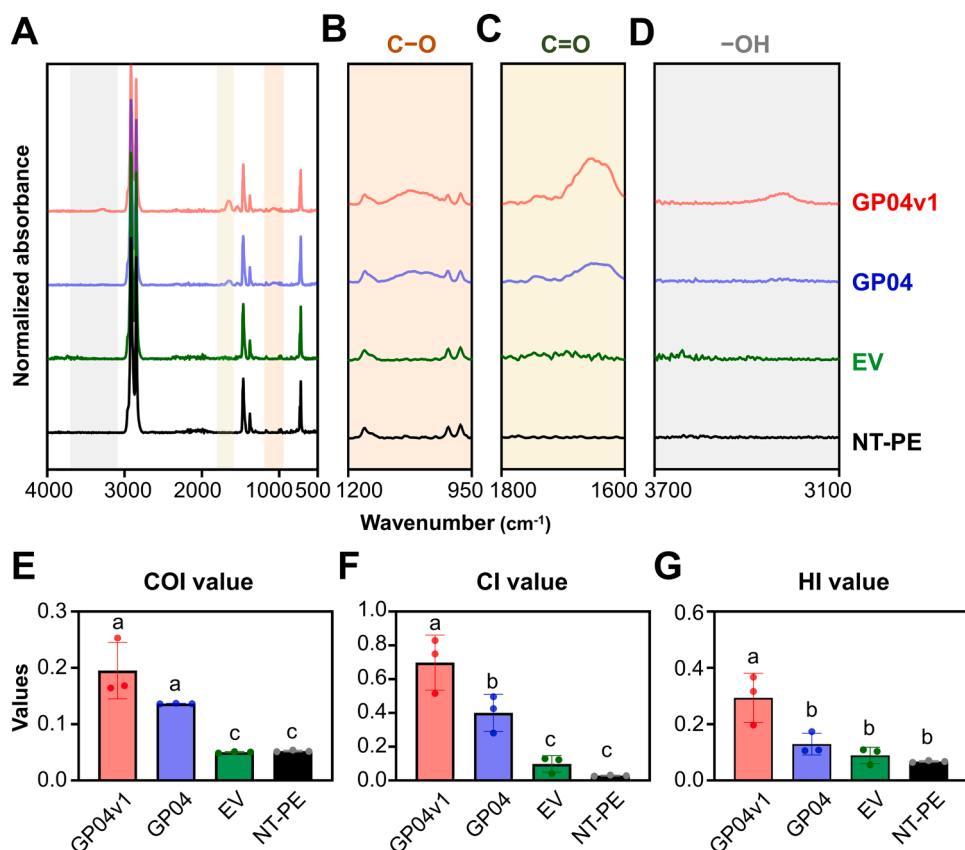


Fig. 6. Enhancement of PE-oxidizing efficiency of CYP6B2-GP04 using directed evolution. (A) FTIR spectrum ($4000\text{--}500\text{ cm}^{-1}$) of PE films after their reaction with CYP6B2-GP04v1 and CYP6B2GP04. The beige-colored area indicates the wavenumber range of $1200\text{--}950\text{ cm}^{-1}$, in which C–O bonds were identified. The sage-colored area highlights the wavenumber range of $1800\text{--}1600\text{ cm}^{-1}$, which indicates the presence of C=O bonds. The gray-colored area indicates the wavenumber range of $3700\text{--}3100\text{ cm}^{-1}$, which corresponds to the detection of hydroxyl bond (–OH). (E–G). Bar graph representing the COI (E), CI (F), and hydroxy index (HI) (G) values, calculated based on the FTIR spectrum (H, I). One-way analysis of variance (ANOVA) was performed using the Tukey's honestly significant difference (HSD) test. Different letters indicate statistically significant differences ($P \leq 0.05$).

Certain insects belonging to the orders Lepidoptera and Coleoptera have been phenotypically reported to degrade PE; however, specific enzymes involved in PE oxidation have not been well-characterized to date [23, 25, 26, 28, 31, 76–78]. Using a combination of reverse and forward genetic approaches, we discovered two PE-oxidizing CYP enzymes CYP6B2-GP04 and CYP6B2-13G08. We then validated their efficiencies through heterologous expression in yeast and insect cells. Furthermore, we performed *in silico* structural analysis and directed evolution on the CYP6B2-GP04 enzyme, which exhibited higher PE oxidation activity, to predict a potential PE oxidation mechanism.

We previously found that *G. mellonella* can oxidize beeswax without the aid of gut microbiota. Here, we demonstrated that *G. mellonella* possesses intestinal enzymes capable of rapidly oxidizing PE polymers within a single digestive cycle from ingestion to excretion in less than 4 h. In 2022 and 2023, four hexamerins (Demetra, Cibeles, Ceres, and Cora) belonging to the hemocyanin/phenoloxidase family were isolated from the *G. mellonella* saliva and proposed to be PE-oxidizing enzymes [36, 38]. When each hexamerin was applied to PE three times for 90 minutes, C–O and C=O bonds formed within the PE polymer, and C₁₀–C₂₂ ketones were produced as byproducts. However, prior studies did not confirm PE oxidation *in vivo*, i.e., they did not characterize the PE oxidation rate in the anterior part of the foregut. In addition, since the salivary glands are directly connected to the mouth and ingested PE is rapidly transferred from the mouth to the digestive tract, saliva-derived enzymes cannot efficiently oxidize PE *in vivo*. Our results showed that ingested PE is primarily oxidized in the midgut, followed by the hindgut, rather than the foregut (Fig. 1B–E). In addition, treating PE with saliva-derived enzymes for 90 min three times *in vitro*, with each treatment using fresh enzymes, takes considerably longer time than the actual *in vivo* conditions. Indeed, our observation indicated that ingested PE swiftly moves to the midgut within 1 h and to the hindgut within 2 h (Fig. S1A). Collectively, these findings indicate that although saliva-derived hexamerins could partially contribute to PE oxidation in *G. mellonella*, the primary oxidation is mediated by gut-derived proteins, such as CYP6B2 enzymes.

CYP6-family enzymes are unique to insects and primarily known to metabolize exogenous substances [39, 40, 45]. Several studies have shown that CYP6 enzymes detoxify allelochemicals and pesticides in herbivorous lepidopteran species [39–41]. In this study, we additionally identified a novel function of the CYP6 family in PE oxidation (Fig. 2E and Fig. 4E). Phylogenetic analyses revealed that the *G. mellonella* CYP6B2 forms a distinct group from other lepidopterans but clusters with *A. grisella*, which also feeds on beeswax composed of long-chain hydrocarbons (Fig. S6). This result indicates that CYP6B2 in both species has uniquely evolved the capacity to metabolize long-chain hydrocarbons. *In silico* structural analysis provided insights into the PE oxidation mechanism by the CYP6B2-GP04. Although the precise structure of the insect CYP6B2 protein has not been determined, homology modeling based on structurally resolved homologous proteins enabled to predict the active sites and substrate-binding regions of the CYP6B2 protein. In CYP enzymes, the substrate is oxidized by an activated oxygen molecule at the heme center. A CYP6B2-GP04 Cys450Ala mutant, which is predicted to lack heme owing to the substitution impairing the heme-binding site, cannot oxidize PE. The requirement of heme in CYP6B2-GP04 for PE oxidation suggests that heme is essential for enabling PE oxidation. Additionally, substrate oxidation efficiency is determined by the interaction energy with surrounding key residues and substrate positioning. Molecular docking simulations revealed that the interaction energy decreases as the hydrocarbon chain length increases, suggesting that PE, a long and complex hydrocarbon, can strongly bind CYP6B2-GP04. Additionally, seven residues were identified as crucial for binding to PE, with Phe118 being the most important among them. Identifying key residues provides essential insights into the mechanism of PE oxidation and establishes a basis for improving PE oxidation efficiency.

We exploited this possibility by performing directed enzyme

evolution to enhance the PE oxidation activity of CYP6B2-GP04. This led to the discovery of CYP6B2-GP04v1 with improved PE oxidation activity. However, *in silico* molecular docking simulations revealed that the difference in interaction energy between CYP6B2-GP04 and CYP6B2-GP04v1 was not significant. The observed discrepancy might be due to the lack of precise structural information, indicating that accurate structural characterization is required. Upon binding CYP, PE undergoes oxidation that occurs in three steps [79]. First, the redox potential of the iron within heme changes upon interaction with a hydrocarbon, leading to an influx of electrons. The resulting electron influx forms a chemically unstable ferryl intermediate, such as a porphyrin radical cation Fe (IV) species, which then oxidizes the hydrocarbons by introducing oxygen into the chain and producing alcohols. The detection of short aliphatic compounds with hydroxyl groups at both ends, such as diglycerol and 4-hydroxybutanoic acid, indicates that oxidation by the *G. mellonella* CYP6B2-GP04 enzyme occurs both at the terminal parts and within the PE polymer chain (Fig. 4F). The ability of the CYP6B2-GP04 enzyme to oxidize PE at multiple points within the polymer chain capability would enable *G. mellonella* to metabolize PE more rapidly and efficiently. As observed in our previous findings with beeswax, the oxidized form of PE by CYP6B2-GP04 and CYP6B2-13G08 could be further metabolized through the fatty acid metabolic pathway in *G. mellonella* [29].

While the discovery of CYP6B2-GP04 and CYP6B2-13G08 enzymes opens new possibilities for biological PE oxidation, our study also has limitations, including a lack of comprehensive understanding of the PE oxidation mechanism by CYP6B2-GP04 and CYP6B2-13G08 enzymes and their practical application in PE biodegradation. Future studies should employ advanced techniques such as cryo-electron microscopy or X-ray crystallography to elucidate the three-dimensional structure and substrate interactions of CYP6B2-GP04 and CYP6B2-13G08. In addition, determining the precise localization of these enzymes within the gut of *G. mellonella* is essential for understanding their functional role in PE oxidation. CYP enzymes are typically located in the endoplasmic reticulum or the inner mitochondrial membrane, and are not secreted outside the cell. The intracellular localization of CYP enzymes poses challenges in explaining how these enzymes can directly interact with PE in the gut. Alternatively, different CYP6-family enzymes may exhibit different subcellular localization, given their unique evolutionary path in insects, although there is no direct evidence. Immunostaining using specific antibodies, along with immune-gold staining TEM, could provide valuable insights into the localization of these enzymes. Last, studies on mass production and purification of CYP6B2-GP04 and CYP6B2-13G08 enzymes would be essential for practical applications in plastic waste management. While expression in *P. pastoris* and insect Sf9 cells provides a foundation, scaling up will require optimization of production conditions and purification methods. Successfully addressing production and purification challenges could pave the way for eco-friendly solutions for PE waste treatment and upcycling. Additionally, further research is needed to investigate the potential involvement of other enzymes in PE oxidation. While our study focused on CYP6B2-GP04 and CYP6B2-13G08, additional enzymes, such as hexamerins discovered in the salivary gland, may contribute to this process, each with distinct mechanisms [36, 38]. Exploring these enzymes and understanding their roles in biological PE oxidation will be another important direction for future research.

In conclusion, our findings demonstrate that *G. mellonella* can rapidly and efficiently oxidize PE using gut-derived enzymes, particularly those from CYP6-family enzymes. The discovery of CYP6B2-GP04 and CYP6B2-13G08 in the gut of *G. mellonella* offers new perspectives for studying additional insect-derived enzymes for PE oxidation. In addition, successful heterologous expression of *G. mellonella* CYP enzymes in yeast cells establishes an efficient screening system for identifying insect-derived PE-oxidizing enzymes. We propose extending the screening approach developed in this study to other insects, such as *T. monitor* and *Z. atratus*, which have also been reported to oxidize PE. Extensive application of this method could uncover novel enzymes and

enhance our understanding of PE oxidation by insects.

Environmental Implication

Polyethylene is a major environmental challenge due to its resistance to degradation. *Galleria mellonella* has enzymes that can oxidize PE, making them valuable for developing biological solutions to plastic waste. This study used heterologous expression systems, including *Pichia pastoris* and insect SF9 cells, to successfully identify two PE-oxidizing enzymes CYP6B2-GP04 and CYP6B2-13G08 from *G. mellonella* and to be able mass production. The identification of the enzymes is particularly noteworthy as the first discovery of insect intestinal PE-oxidizing enzymes. These enzymes offer a novel, eco-friendly solution to plastic waste management, addressing the growing environmental concerns associated with polyethylene pollution.

Funding

This work was supported by the Cooperative Research Program for Agriculture Science & Technology Development (Project No. RS-2020-RD009221) of the Rural Development Administration and by the Korea Research Institute of Bioscience and Biotechnology (KRIBB) Research Initiative Program (KGM9942421 and KGM5322422).

CRediT authorship contribution statement

Jin-Soo Son: Writing – original draft, Visualization, Validation, Methodology, Investigation, Formal analysis, Conceptualization. **Soo-hyun Lee:** Resources, Investigation, Conceptualization. **Sungbo Hwang:** Software, Formal analysis, Data curation. **Jinyoung Jeong:** Methodology, Funding acquisition, Formal analysis. **Seonghan Jang:** Writing – original draft, Visualization, Software, Formal analysis, Data curation. **Jiyoung Gong:** Methodology. **Jae Young Choi:** Resources, Formal analysis. **Youn Ho Je:** Resources. **Choong-Min Ryu:** Writing – review & editing, Supervision, Project administration, Funding acquisition, Conceptualization.

Declaration of Competing Interest

The authors declare that they have no known competing financial interests or personal relationships that could have appeared to influence the work reported in this paper.

Appendix A. Supporting information

Supplementary data associated with this article can be found in the online version at [doi:10.1016/j.jhazmat.2024.136264](https://doi.org/10.1016/j.jhazmat.2024.136264).

Data Availability

The data that has been used is confidential.

References

- [1] Sivan, A., 2011. New perspectives in plastic biodegradation. *Curr Opin Biotechnol* 22 (3), 422–426. <https://doi.org/10.1016/j.copbio.2011.01.013>.
- [2] Jambeck, J.R., Geyer, R., Wilcox, C., Siegler, T.R., Perryman, M., Andrady, A., et al., 2015. Plastic waste inputs from land into the ocean. *Science* 347 (6223), 768–771. <https://doi.org/10.1126/science.126035>.
- [3] Geyer, R., Jambeck, J.R., Law, K.L., 2017. Production, use, and fate of all plastics ever made. *Sci Adv* 3 (7), e1700782. <https://doi.org/10.1126/sciadv.1700782>.
- [4] Lebreton, L., Andrady, A., 2019. Future scenarios of global plastic waste generation and disposal. *Palgrave Commun* 5 (1), 1–11. <https://doi.org/10.1057/s41599-018-0212-7>.
- [5] PlasticsEurope., 2016. Plastics—The Facts 2016. An analysis of European latest plastics production, demand and waste data. (<https://plasticseurope.org/knowledge-hub/plastics-the-facts-2016/>).
- [6] OECD, 2022. Modelling approaches used to compose the OECD Global Plastics Outlook Database. <https://doi.org/10.1787/c2744069-en>.
- [7] Gourmelon, G., 2015. Global plastic production rises, recycling lags. *Vital Signs* 22, 91–95. (<http://www.worldwatch.org/global-plastic-production-rises-recycling-lags-0>).
- [8] Hopewell, J., Dvorak, R., Kosior, E., 2009. Plastics recycling: challenges and opportunities. *Philos Trans R Soc B: Biol Sci* 364 (1526), 2115–2126. <https://doi.org/10.1098/rstb.2008.0311>.
- [9] U.S. Environmental Protection Agency, 2018. Advancing Sustainable Materials Management: 2015 Tables and Figures. (<https://www.epa.gov/facts-and-figures-about-materials-waste-and-recycling/advancing-sustainable-materials-management>).
- [10] Yao, Z., Seong, H.J., Jang, Y.-S., 2022. Environmental toxicity and decomposition of polyethylene. *Ecotoxicol Environ Saf* 242, 113933. <https://doi.org/10.1016/j.ecoenv.2022.113933>.
- [11] Verma, R., Vinoda, K., Papireddy, M., Gowda, A., 2016. Toxic pollutants from plastic waste—a review. *Procedia Environ Sci* 35, 701–708. <https://doi.org/10.1016/j.proenv.2016.07.069>.
- [12] Ammala, A., Bateman, S., Dean, K., Petinakis, E., Sangwan, P., Wong, S., et al., 2011. An overview of degradable and biodegradable polyolefins. *Prog Polym Sci* 36 (8), 1015–1049. <https://doi.org/10.1016/j.proenv.2016.07.069>.
- [13] Vert, M., Doi, Y., Hellwich, K.-H., Hess, M., Hodge, P., Kubisa, P., et al., 2012. Terminology for biorelated polymers and applications (IUPAC Recommendations 2012). *Pure Appl Chem* 84 (2), 377–410. <https://doi.org/10.1351/PAC-REC-10-12-04>.
- [14] Moshood, T.D., Nawanir, G., Mahmud, F., Mohamad, F., Ahmad, M.H., AbdulGhani, A., 2022. Sustainability of biodegradable plastics: new problem or solution to solve the global plastic pollution? *Curr Res Green Sustain Chem* 5, 100273. <https://doi.org/10.1016/j.crgsc.2022.100273>.
- [15] Yoshida, S., Hiraga, K., Takehana, T., Taniguchi, I., Yamaji, H., Maeda, Y., et al., 2016. A bacterium that degrades and assimilates poly (ethylene terephthalate). *Science* 351 (6278), 1196–1199. <https://doi.org/10.1126/science.1260359>.
- [16] Zheng, Y., Yanful, E.K., Bassi, A.S., 2005. A review of plastic waste biodegradation. *Crit Rev Biotechnol* 25 (4), 243–250. <https://doi.org/10.1080/07388550500346359>.
- [17] Amobonye, A., Bhagwat, P., Singh, S., Pillai, S., 2021. Plastic biodegradation: Frontline microbes and their enzymes. *Sci Total Environ* 759, 143536. <https://doi.org/10.1016/j.scitotenv.2020.143536>.
- [18] Zhang, Y., Pedersen, J.N., Eser, B.E., Guo, Z., 2022. Biodegradation of polyethylene and polystyrene: From microbial deterioration to enzyme discovery. *Biotechnol Adv* 60, 107991. <https://doi.org/10.1016/j.biotechadv.2022.107991>.
- [19] Ghatge, S., Yang, Y., Ahn, J.-H., Hur, H.-G., 2020. Biodegradation of polyethylene: a brief review. *Appl Biol Chem* 63, 1–14. <https://doi.org/10.1186/s13765-020-00511-3>.
- [20] Yun, S.-D., Lee, C.O., Kim, H.-W., An, S.J., Kim, S., Seo, M.-J., et al., 2023. Exploring a New Biocatalyst from *Bacillus thuringiensis* JNU01 for Polyethylene Biodegradation. *Environ Sci Technol Lett* 10 (6), 485–492. <https://doi.org/10.1021/acs.estlett.3c00189>.
- [21] Zhang, J., Gao, D., Li, Q., Zhao, Y., Li, L., Lin, H., et al., 2020. Biodegradation of polyethylene microplastic particles by the fungus *Aspergillus flavus* from the guts of wax moth *Galleria mellonella*. *Sci Total Environ* 704, 135931. <https://doi.org/10.1016/j.scitotenv.2019.135931>.
- [22] El-Sayed, M.T., Rabie, G.H., Hamed, E.A., 2021. Biodegradation of low-density polyethylene (LDPE) using the mixed culture of *Aspergillus carbonarius* and *A. fumigatus*. *Environ, Dev Sustain* 1–29. <https://doi.org/10.1007/s10668-021-01258-7>.
- [23] Peng, B.-Y., Li, Y., Fan, R., Chen, Z., Chen, J., Brandon, A.M., et al., 2020. Biodegradation of low-density polyethylene and polystyrene in superworms, larvae of *Zophobas atratus* (Coleoptera: Tenebrionidae): Broad and limited extent depolymerization. *Environ Pollut* 266, 115206. <https://doi.org/10.1016/j.envpol.2020.115206>.
- [24] Peng, B.-Y., Sun, Y., Wu, Z., Chen, J., Shen, Z., Zhou, X., et al., 2022. Biodegradation of polystyrene and low-density polyethylene by *Zophobas atratus* larvae: Fragmentation into microplastics, gut microbiota shift, and microbial functional enzymes. *J Clean Prod* 367, 132987. <https://doi.org/10.1016/j.jclepro.2022.132987>.
- [25] Yang, Y., Wang, J., Xia, M., 2020. Biodegradation and mineralization of polystyrene by plastic-eating superworms *Zophobas atratus*. *Sci Total Environ* 708, 135233. <https://doi.org/10.1016/j.scitotenv.2019.135233>.
- [26] Brandon, A.M., Gao, S.-H., Tian, R., Ning, D., Yang, S.-S., Zhou, J., et al., 2018. Biodegradation of polyethylene and plastic mixtures in mealworms (larvae of *Tenebrio molitor*) and effects on the gut microbiome. *Environ Sci Technol* 52 (11), 6526–6533. <https://doi.org/10.1021/acs.est.8b02301>.
- [27] Bilal, H., Raza, H., Bibi, H., Bibi, T., 2021. Plastic biodegradation through insects and their symbionts microbes: a review. *J Bioresour Manag* 8 (4). <https://doi.org/10.35691/JBM.1202.0206>.
- [28] Bombelli, P., Howe, C.J., Bertocchini, F., 2017. Polyethylene bio-degradation by caterpillars of the wax moth *Galleria mellonella*. *Curr Biol* 27 (8), R292–R293. <https://doi.org/10.1016/j.cub.2017.02.060>.
- [29] Kong, H.G., Kim, H.H., Chung, J.-h., Jun, J., Lee, S., Kim, H.-M., et al., 2019. The *Galleria mellonella* hologenome supports microbiota-independent metabolism of long-chain hydrocarbon beeswax. *e2455 Cell Rep* 26 (9), 2451–2464. <https://doi.org/10.1016/j.celrep.2019.02.018>.
- [30] Latour, S., Noël, G., Serteyn, L., Sare, A.R., Massart, S., Delvigne, F., Francis, F., 2021. Multi-omics approach reveals new insights into the gut microbiome of *Galleria mellonella* (Lepidoptera: Pyralidae) exposed to polyethylene diet, 2006. 2004.446152 bioRxiv 2021. <https://doi.org/10.1101/2021.06.04.446152>.

- [31] Yang, J., Yang, Y., Wu, W.-M., Zhao, J., Jiang, L., 2014. Evidence of polyethylene biodegradation by bacterial strains from the guts of plastic-eating waxworms. *Environ Sci Technol* 48 (23), 13776–13784. <https://doi.org/10.1021/es504038a>.
- [32] LeMoine, C.M., Grove, H.C., Smith, C.M., Cassone, B.J., 2020. A very hungry caterpillar: polyethylene metabolism and lipid homeostasis in larvae of the greater wax moth (*Galleria mellonella*). *Environ Sci Technol* 54 (22), 14706–14715. <https://doi.org/10.1021/acs.est.0c04386>.
- [33] Lou, Y., Ekaterina, P., Yang, S.-S., Lu, B., Liu, B., Ren, N., et al., 2020. Biodegradation of polyethylene and polystyrene by greater wax moth larvae (*Galleria mellonella* L.) and the effect of co-diet supplementation on the core gut microbiome. *Environ Sci Technol* 54 (5), 2821–2831. <https://doi.org/10.1021/acs.est.9b07044>.
- [34] Montazer, Z., Habibi Najafi, M.B., Levin, D.B., 2021. *In vitro* degradation of low-density polyethylene by new bacteria from larvae of the greater wax moth, *Galleria mellonella*. *Can J Microbiol* 67 (3), 249–258. <https://doi.org/10.1139/cjm-2020-0208>.
- [35] Ruiz Barrionuevo, J.M., Vilanova-Cuevas, B., Galindo-Cardona, A., Monmany-Garza, A., Godoy-Vitorino, F., 2022. The bacterial and fungal gut microbiota of the greater wax moth, *Galleria mellonella* L. consuming polyethylene and polystyrene. *Front Microbiol* 13, 918861. <https://doi.org/10.3389/fmicb.2022.918861>.
- [36] Sanluis-Verdes, A., Colomer-Vidal, P., Rodríguez-Ventura, F., Bello-Villarino, M., Spínola-Amilibia, M., Ruiz-López, E., et al., 2022. Wax worm saliva and the enzymes therein are the key to polyethylene degradation by *Galleria mellonella*. *Nat Commun* 13 (1), 1–11. <https://doi.org/10.1038/s41467-022-33127-w>.
- [37] Kesti, S.S.K., Thimmappa, S.C.T., 2019. First report on biodegradation of low density polyethylene by rice moth larvae, *Coryca cephalonica* (Stainton). *Holist Approach Environ* 9 (4), 79–83. <https://doi.org/10.33765/thate.9.4.2>.
- [38] Spínola-Amilibia, M., Illanes-Vicioso, R., Ruiz-López, E., Colomer-Vidal, P., Rodríguez-Ventura, F., Peces Pérez, R., et al., 2023. Plastic degradation by insect hexamerins: Near-atomic resolution structures of the polyethylene-degrading proteins from the wax worm saliva. *Sci Adv* 9 (38), eadi6813. <https://doi.org/10.1126/sciadv.adi6813>.
- [39] Scott, J.G., 1999. Cytochromes P450 and insecticide resistance. *Insect Biochem Mol Biol* 29 (9), 757–777. [https://doi.org/10.1016/s0965-1748\(99\)00038-7](https://doi.org/10.1016/s0965-1748(99)00038-7).
- [40] Feyereisen, R., 1999. Insect P450 enzymes. *Annu Rev Entomol* 44 (1), 507–533. <https://doi.org/10.1146/annurev.ento.44.1.507>.
- [41] Feyereisen, R., 2012. Insect CYP genes and P450 enzymes. *Insect molecular biology and biochemistry*. Elsevier, pp. 236–316. <https://doi.org/10.1016/B978-0-12-384747-8.10008-X>.
- [42] Nauen, R., Bass, C., Feyereisen, R., Vontas, J., 2022. The role of cytochrome P450s in insect toxicology and resistance. *Annu Rev Entomol* 67, 105–124. <https://doi.org/10.1146/annurev-ento-070621-061328>.
- [43] Krieger, R.L., Feeny, P.P., Wilkinson, C.F., 1971. Detoxication enzymes in the guts of caterpillars: an evolutionary answer to plant defenses? *Science* 172 (3983), 579–581. <https://doi.org/10.1126/science.172.3983.579>.
- [44] Dermauw, W., Van Leeuwen, T., Feyereisen, R., 2020. Diversity and evolution of the P450 family in arthropods. *Insect Biochem Mol Biol* 127, 103490. <https://doi.org/10.1016/j.ibmb.2020.103490>.
- [45] Feyereisen, R., 2006. Evolution of insect P450. *Biochem Soc Trans* 1866:141–154. <https://doi.org/10.1042/BST0341252>.
- [46] Wang, H., Shi, Y., Wang, L., Liu, S., Wu, S., Yang, Y., et al., 2018. CYP6AE gene cluster knockout in *Helicoverpa armigera* reveals role in detoxification of phytochemicals and insecticides. *Nat Commun* 9 (1), 4820. <https://doi.org/10.1038/s41467-018-07226-6>.
- [47] Ranasinghe, C., Headlam, M., Hobbs, A.A., 1997. Induction of the mRNA for CYP6B2, a pyrethroid inducible cytochrome P450, in *Helicoverpa armigera* (Hubner) by dietary monoterpenes. *Arch Insect Biochem Physiol* 34 (1), 99–109. [https://doi.org/10.1002/\(SICI\)1520-6327\(1997\)34:1<99::AID-ARCH8-3.0.CO;2-R](https://doi.org/10.1002/(SICI)1520-6327(1997)34:1<99::AID-ARCH8-3.0.CO;2-R).
- [48] Vontas, J., Katsavou, E., Mavridis, K., 2020. Cytochrome P450-based metabolic insecticide resistance in *Anopheles* and *Aedes* mosquito vectors: Muddying the waters. *Pestic Biochem Physiol* 170, 104666. <https://doi.org/10.1016/j.pestbp.2020.104666>.
- [49] Wang, J., Wang, Y., Li, X., Weng, Y., Dong, X., Zhao, X., 2022. Comparison on the effectiveness of Fourier transform infrared (FT-IR) and attenuated total reflection Fourier transform infrared (ATR-FT-IR) in characterizing plastics biodegradation by insect larvae. *Sci Total Environ* 839, 156289. <https://doi.org/10.1016/j.scitotenv.2022.156289>.
- [50] Sanger, P.-A., Wagner, S., Liebler-Tenorio, E.M., Fuchs, T.M., 2022. Dissecting the invasion of *Galleria mellonella* by *Yersinia enterocolitica* reveals metabolic adaptations and a role of a phage lysis cassette in insect killing. *PLoS Pathog* 18 (11), e1010991. <https://doi.org/10.1371/journal.ppat.1010991>.
- [51] Almond, J., Sugumaar, P., Wenzel, M.N., Hill, G., Wallis, C., 2020. Determination of the carbonyl index of polyethylene and polypropylene using specified area under band methodology with ATR-FTIR spectroscopy. *e-Polym* 20 (1), 369–381. <https://doi.org/10.1515/epoly-2020-0041>.
- [52] Campanaro, A.L., Simcik, M.F., Maurer-Jones, M.A., Penn, R.L., 2023. Sewage sludge induces changes in the surface chemistry and crystallinity of polyalactic acid and polyethylene films. *Sci Total Environ* 890, 164313. <https://doi.org/10.1016/j.scitotenv.2023.164313>.
- [53] Zhang, Z., Peng, H., Yang, D., Zhang, G., Zhang, J., Ju, F., 2022. Polyvinyl chloride degradation by a bacterium isolated from the gut of insect larvae. *Nat Commun* 13 (1), 5360. <https://doi.org/10.1038/s41467-022-32903-y>.
- [54] Abramson, J., Adler, J., Dunger, J., Evans, R., Green, T., Pritzel, A., et al., 2024. Accurate structure prediction of biomolecular interactions with AlphaFold 3. *Nature* 630, 493–500. <https://doi.org/10.1038/s41586-024-07487-w>.
- [55] Abraham, M.J., Murtola, T., Schulz, R., Pall, S., Smith, J.C., Hess, B., Lindahl, E., 2015. GROMACS: High performance molecular simulations through multi-level parallelism from laptops to supercomputers. *SoftwareX* 1 19–25. <https://doi.org/10.1016/j.softx.2015.06.001>.
- [56] Jo, S., Kim, T., Iyer, V.G., Im, W., 2008. CHARMM-GUI: a web-based graphical user interface for CHARMM. *J Comput Chem* 29 (11), 1859–1865. <https://doi.org/10.1002/jcc.20945>.
- [57] Kim, S., Chen, J., Cheng, T., Gindulyte, A., He, J., He, S., et al., 2023. PubChem 2023 update. *Nucleic Acids Res* 51 (D1), D1373–D1380. <https://doi.org/10.1093/nar/gkac956>.
- [58] Eberhardt, J., Santos-Martins, D., Tillack, A.F., Forli, S., 2021. AutoDock Vina 1.2.0: New docking methods, expanded force field, and python bindings. *J Chem Inf Model* 61 (8), 3891–3898. <https://doi.org/10.1021/acs.jcim.1c00203>.
- [59] Trott, O., Olson, A.J., 2010. AutoDock Vina: improving the speed and accuracy of docking with a new scoring function, efficient optimization, and multithreading. *J Comput Chem* 31 (2), 455–461. <https://doi.org/10.1002/jcc.21334>.
- [60] Morris, G.M., Huey, R., Lindstrom, W., Sanner, M.F., Belew, R.K., Goodsell, D.S., Olson, A.J., 2009. AutoDock4 and AutoDockTools4: Automated docking with selective receptor flexibility. *J Comput Chem* 30 (16), 2785–2791. <https://doi.org/10.1002/jcc.21256>.
- [61] Pettersen, E.F., Goddard, T.D., Huang, C.C., Couch, G.S., Greenblatt, D.M., Meng, E.C., Ferrin, T.E., 2004. UCSF Chimera—a visualization system for exploratory research and analysis. *J Comput Chem* 25 (13), 1605–1612. <https://doi.org/10.1002/jcc.20084>.
- [62] Kitaura, K., Ikeo, E., Asada, T., Uebayasi, M., 1999. Fragment molecular orbital method: an approximate computational method for large molecules. *Chem Phys Lett* 313 (3–4), 701–706. [https://doi.org/10.1016/S0009-2614\(99\)00874-X](https://doi.org/10.1016/S0009-2614(99)00874-X).
- [63] Fedorov, D.G., Kitaura, K., 2007. Extending the power of quantum chemistry to large systems with the fragment molecular orbital method. *J Phys Chem A* 111 (30), 6904–6914. <https://doi.org/10.1021/jp0716740>.
- [64] Gaus, M., Cui, Q., Elstner, M., 2011. DFTB3: Extension of the self-consistent-charge density-functional tight-binding method (SCC-DFTB). *J Chem Theory Comput* 7 (4), 931–948. <https://doi.org/10.1021/ct100684s>.
- [65] Nakano, T., Kaminuma, T., Sato, T., Akiyama, Y., Uebayasi, M., Kitaura, K., 2000. Fragment molecular orbital method: application to polypeptides. *Chem Phys Lett* 318 (6), 614–618. [https://doi.org/10.1016/S0009-2614\(00\)00070-1](https://doi.org/10.1016/S0009-2614(00)00070-1).
- [66] Tomasi, J., Mennucci, B., Cammi, R., 2005. Quantum mechanical continuum solvation models. *Chem Rev* 105 (8), 2999–3094. <https://doi.org/10.1021/cr9904009>.
- [67] Barca, G.M., Bertoni, C., Carrington, L., Datta, D., De Silva, N., Deustua, J.E., et al., 2020. Recent developments in the general atomic and molecular electronic structure system. *J Chem Phys* 152 (15). <https://doi.org/10.1063/5.0005188>.
- [68] Kalish, J.E., Chen, C.L., Gould, S.J., Watkins, P.A., 1995. Peroxisomal activation of long-and very long-chain fatty acids in the yeast *Pichia pastoris*. *Biochem Biophys Res Commun* 206 (1), 335–340. <https://doi.org/10.1006/bbrc.1995.1046>.
- [69] Ferdinandusse, S., Denis, S., Hogenhout, E.M., Koster, J., Van Roermund, C.W., IJlst, L., et al., 2007. Clinical, biochemical, and mutational spectrum of peroxisomal acyl-coenzyme A oxidase deficiency. *Hum Mutat* 28 (9), 904–912. <https://doi.org/10.1002/humu.20535>.
- [70] Oaxaca-Castillo, D., Andreoletti, P., Vluggens, A., Yu, S., Van Veldhoven, P.P., Reddy, J.K., Cherkaoui-Malki, M., 2007. Biochemical characterization of two functional human liver acyl-CoA oxidase isoforms 1a and 1b encoded by a single gene. *Biochem Biophys Res Commun* 360 (2), 314–319. <https://doi.org/10.1016/j.bbrc.2007.06.059>.
- [71] Schmitz, G., Kaminski, W., 2002. ABCA2: a candidate regulator of neural transmembrane lipid transport. *Cell Mol Life Sci CMLS* 59, 1285–1295. <https://doi.org/10.1007/s00018-002-8508-5>.
- [72] Morita, M., Imanaka, T., 2012. Peroxisomal ABC transporters: structure, function and role in disease. *Biochim Et Biophys Acta (BBA)-Mol Basis Dis* 1822 (9), 1387–1396. <https://doi.org/10.1016/j.bbadis.2012.02.009>.
- [73] Butovich, I.A., Wilkerson, A., Goggans, K.R., Belyaeva, O.V., Kedishvili, N.Y., Yuksel, S., 2023. *Sdr16c5* and *Sdr16c6* control a dormant pathway at a bifurcation point between meibogenesis and sebogenesis. *J Biol Chem* 299 (6). <https://doi.org/10.1016/j.jbc.2023.104725>.
- [74] Scott, J.G., Liu, N., Wen, Z., 1998. Insect cytochromes P450: diversity, insecticide resistance and tolerance to plant toxins. *Comp Biochem Physiol Part C: Pharmacol, Toxicol Endocrinol* 121 (1–3), 147–155. [https://doi.org/10.1016/S0742-8413\(98\)10035-X](https://doi.org/10.1016/S0742-8413(98)10035-X).
- [75] Yeom, S.-J., Le, T.-K., Yun, C.-H., 2022. P450-driven plastic-degrading synthetic bacteria. *Trends Biotechnol* 40 (2), 166–179. <https://doi.org/10.1016/j.tibttech.2021.06.003>.
- [76] Peng, B.-Y., Xu, Y., Sun, Y., Xiao, S., Sun, J., Shen, Z., et al., 2023. Biodegradation of polyethylene (PE) microplastics by mealworm larvae: Physiological responses, oxidative stress, and residual plastic particles. *J Clean Prod* 402, 136831. <https://doi.org/10.1016/j.jclepro.2023.136831>.
- [77] Peng, B.-Y., Su, Y., Chen, Z., Chen, J., Zhou, X., Benbow, M.E., et al., 2019. Biodegradation of polystyrene by dark (*Tenebrio obscurus*) and yellow (*Tenebrio molitor*) mealworms (Coleoptera: Tenebrionidae). *Environ Sci Technol* 53 (9), 5256–5265. <https://doi.org/10.1021/acs.est.8b06963>.
- [78] Kundungal, H., Gangarapu, M., Sarangapani, S., Patchaiyappan, A., Devipriya, S.P., 2019. Efficient biodegradation of polyethylene (HDPE) waste by the plastic-eating lesser waxworm (*Achroia grisella*). *Environ Sci Pollut Res* 26, 18509–18519. <https://doi.org/10.1007/s11356-019-05038-9>.
- [79] Ortiz de Montellano, P.R., 2010. Hydrocarbon hydroxylation by cytochrome P450 enzymes. *Chem Rev* 110 (2), 932–948. <https://doi.org/10.1021/cr9002193o>.

Glossary

PE: Polyethylene

PET: Polyethylene terephthalate

CYP: Cytochrome P450 monooxygenase

EV: Empty vector

ATR-FTIR: Attenuated total reflection-Fourier transform infrared spectroscopy

GC-MS: Gas Chromatography-Mass Spectrometry

COG: The clusters of orthologous groups of proteins

COI: Carbon-oxygen index

CI: Carbonyl index

HI: Hydroxyl index

BMGY: Buffered Glycerol-complex broth medium

BMMY: Buffered Methanol-complex broth medium